Universitat
de les Illes Balears

Diurnal moist convection in Majorca under breeze conditions: Idealized numerical experiments

AUTHOR: JAVIER MARTÍN MARTÍN

Master's Thesis

Master's degree in Física Avançada i Matemàtica Aplicada (FAMA)

Especialitat de Fluids Geofisics

at the

UNIVERSITAT DE LES ILLES BALEARS

Academic year 2015-2016

Date 12 /09/ 2016   *Author signature* _____

UIB Master's Thesis Supervisor Dr. Romualdo Romero March __   *Supervisor signature* _____

UIB Master's Thesis Co-Supervisor (if required) _____   *Co-Supervisor signature* ___

ACKNOWLEDGEMENTS

INDEX

INTRODUCTION

1 MESOSCALE PROCESSES

The spatial and temporal scales for which all analyses of this project have been performed is called mesoscale. The geostrophic approach that explains the atmospheric processes that take place in the synoptic scale is not valid for our work, since the horizontal accelerations of the wind break the geostrophic balance between the horizontal pressure gradient and Coriolis force. On the other hand, the vertical accelerations break the hydrostatic equilibrium between the vertical pressure gradient and the gravity acceleration. There is also a frictional term which is not explicitly resolved by the MM5 model, so it has to be parametrized by the boundary layer scheme chosen in the model.

Horizontal motion equation: $\partial_t V + V \nabla V = \frac{1}{\rho} \nabla V + f(k\,x\,v) + \eta \nabla^2 V$

Vertical motion equation: $\partial_t w + w \partial_z w = \frac{1}{\rho} \partial_z V + f(k\,x\,v) + \eta \partial_{zz} V$

where V is the horizontal component of the wind vector, w is the vertical component of the wind vector, ρ is the air density, f is the Coriolis parameter and η is the kinematic viscosity.

The solutions of The 2nd grade Navier-Stokes equations admit numerical solutions. As the spatial and temporal scale of the meteorological processes decrease, a higher resolution is needed in order to define them better. It is important in mesoscale studies to have a high-resolution topography with the aim of resolving the local impact on the forecast, due to the interactions of the fluxes with the relief and the unsteady conditions of the troposphere. Diabatic processes related with the latent heat exchange play an important role as well, which are implicit in the thermodynamic equation that relates these processes with the local and advective variations of the temperature, and the stability.

Thermodynamics equation: $$[\partial_t + V \nabla] T - w S_p = \frac{q}{C_p}$$

where V is the horizontal component of the wind, T is the temperature, w is equal to dp/dt, Sp is the hydrostatic stability parameter, C_p is the heat capacity at constant pressure and q is the temporal latent heating rate.

A multitude of phenomena can be evolve into the atmosphere. On the one hand, there are processes related with stability conditions as mountain waves, downslope winds, radiation fog, etc. On the other hand, convection can lead to various mesoscale processes related with moist instability as supercells, convective systems, squall lines, etc. All these processes depend on the wind shear, which enables the convection to be organized in one way or another, with a minimum value estimated at 10 m/s. Three essential ingredients are needed at the same time in order to develop convection: moisture, instability conditions and a trigger mechanism, at the same time. There are many trigger mechanism as convergence of winds at low levels, orographic forcing, dynamical forcing due to the passage of an upper trough, etc. There are several sources that could generate these convergences at low levels. The area of study is located in the western Mediterranean basin, where the convergence is frequently produced by the predominant northwesterly wind called *Mistral*, or the northern winds called *Tramuntana*. The *Mistral* is reinforced by the orographic dipole developed leewards the Pyrenees, and the *Tramuntana* is developed under a particular synoptic pressure conditions, with low pressure located in northern Italy and high pressures in the southwest of France, synoptic conditions which are frequently occurring due to the ciclogenesis leewards to the Alps, generated by the interaction of the synoptic flow with the mountain range.

This project focus in mesoscale phenomena which are not substantially influence by the synoptic conditions. As opposed to the other Balearic islands, Majorca has a sufficiently large size for developing well-marked sea breeze circulations in all coastal areas of the island, but inducing convergence zones some distance from the coast that tend to propagate inland during the diurnal hours inside.

On 30th of August 2004, convection was detected in the center of Majorca under conditions of instability in the tropospheric column, being the convergence of the sea breeze the triggering mechanism. This event was the main motivation in order to establish the basis for this project.

It is convenient to have a prior knowledge of some studies that have been done on the sea breeze in Majorca, before going into detail with the description of this project.

The first analysis of the sea breeze regime was done by J.M. Jansà and Jaume (1946). They resorted to climatology empirical knowledge of the sea breeze from the field workers and fishermen; a map with the streamlines was plotted from the data collected, locating the main inflows along the Bays of *Palma* and *Alcudia*, and a secondary one in the south, (Fig. 1). The most important feature is they collide in the center, creating a convergence line, the authors also realized that there is a clear influence of the orography on the sea breeze streamlines.
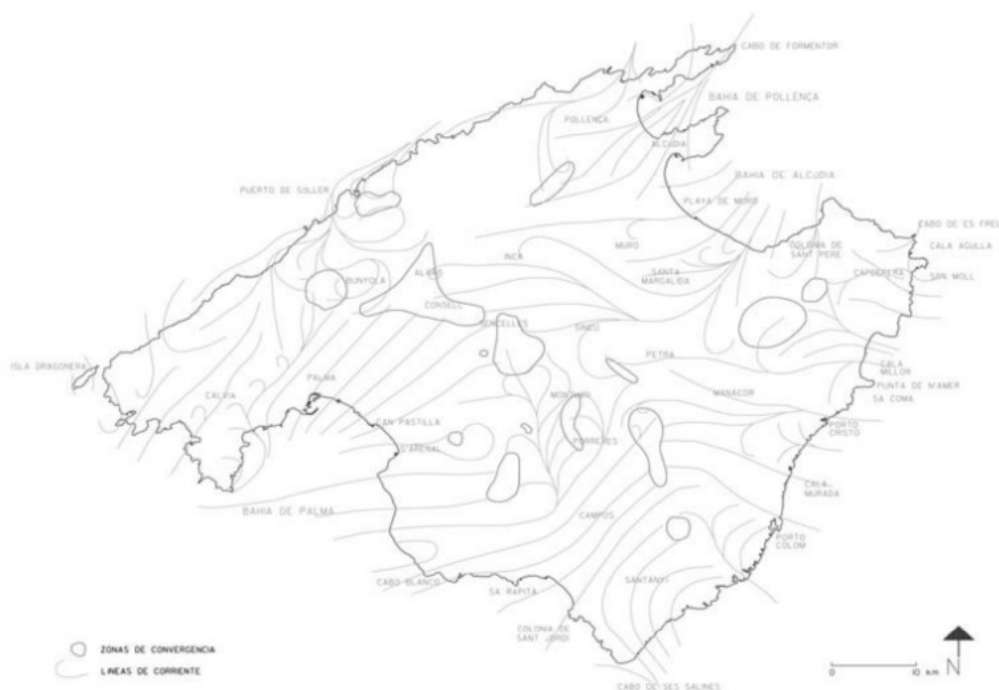

Figure 1. Streamlines of the mature sea breeze and convergence areas over the island of Majorca, based on experimental observations by J.M. Jansà and Jaume (1946). Picture taken from Alomar G. et al. (2004).

Afterwards, an analysis of the existence of areas of convergence from the clouds formations was done by Ramis C. and S. Alonso (1988), using the images of the satellite Meteosat. Two years later, the first numerical simulation of the sea breeze was run with a simple bi-dimensional model, Ramis *et al.* (1990), where an assumption on the acceleration of the wind was made: this acceleration depends on pressure perturbation, which in turn depends on: the temperature anomaly generated by differential heating, the Coriolis force using an alpha plane approximation for 40º and the blocking effect of the orography. In 1995, a sophisticated numerical model was run to simulate the three-dimensional structure of the sea breeze circulation, Ramis C. and R. Romero (1995), obtaining similar results to the experimental observations of Jansà and Jaume (1946). It was also found that the main action of the dryness over the circulation is to enhance the wind all over the coast, in such a way the convergence line in the center of the island does not occur when the soil is wet. It was also suggested the idea of simulate different synoptic fluxes in order to analyse their action over the main features of the breeze. One year later, a numerical study on the transport and diffusion of coastal pollutants during the breeze cycle in the island of Majorca was carried out by Romero R. and C. Ramis (1996). Subsequently, a characterization of the sea breeze of Majorca related with the divergence of the mean wind flow was done by Gonzalez J. *et al.* (1997). The convergence is obtained from three automatic weather stations located strategically in the coast of Majorca. It was found a predominance of convergence during daytime and a predominance of the divergence during nighttime.

In order to continue with the studies that have been carried out by the authors discussed above, we move a step further and analyze in this work how the synoptic wind field interacts with the sea breeze generated by thermal differences during daytime, using the accumulated precipitation field as a tracer. Therefore, a series of idealized initial atmospheres with certain characteristics have been created, in order to isolate as much as possible, the changes that occur in response to the varying synoptic wind field. On the one hand, the vertical temperature and moisture profiles for all the idealized atmospheres have been initialized from the atmospheric sounding launched on 30th of August 2004 at 00z, in the Aerodrome of Son

Bonet (Majorca). On the other hand, all the idealized atmospheres differs from each other in the inclusion of different horizontal wind components (covering all wind directions). A total of thirty-two idealized atmospheres have thus been created in order to be compare the results with respect to a reference atmosphere characterized by resting conditions in the vertical (i.e zero wind). Nevertheless, the characteristics of the idealized atmospheres will be explained in more detail in the methodology section. From the above idealized soundings, the sea breeze cycle has been simulated, once the initial and boundaries conditions have been established, they have been simulated twenty-four hours throughout the day 30th of August 2004, using the non-hydrostatical MM5 numerical model. The accumulated precipitation field obtained after twenty-four hours of simulation is used in order to apply the object oriented verification method developed by Wernli H. *et al.* (2008). The first part of this work is to quantify the differences between each scenario regarding to the control simulation in order to determine how the different initial and boundary wind conditions affect to the development of the convergence areas under sea breeze conditions. Subsequently, due to the fact that the wind flow is influenced by the orography within the island, the thirty-two different idealized atmospheres have been run again with the orography of Majorca set to zero. The aim of this second part is to compare the simulation of each idealized atmosphere taking into account the orography, with its counterpart with the orography set in one meter. Therefore, the object oriented verification method SAL is applied again to these non-orographic simulations in order to quantify the role of the orography.

2 OVERVIEW OF THE REGION

The mean synoptic flow interacts in different ways with the orography depending on the direction and intensity of the wind. So, it is crucial to have in mind the relief of the island in order to understand the results obtained in every scenario of this project.

Majorca is located in the center of the Western Mediterranean, with an extension of 3626 km² (between 39º and 40º N and 2.4º and 3.5ºE). The high relief of the *Serra of Tramuntana* is located in the west and northwest, with the highest point of 1440 m at Puig Major; Serra of Levante is located in the east, reaching up 500 m above sea level, and there is a central lowland plateau which connects the two main bays situated in the north-east (Bay of *Alcudia*) and south-west (Bay of *Palma*). The coast is mainly smooth except in the north-west due to the presence of the *Serra of Tramuntana*. If we focus on the streamlines, the sea breeze is located as follows: NE on the Bays of *Pollenca* and *Alcudia,* E-SE on the coast of *Levante*, SW mainly on the Bay of *Palma*.

3 SEA BREEZE CIRCULATION CIRULATION

The sea breeze is a thermally-forced circulation typical of the warm season of the year. It is particularly known in Mallorca as "*embat*" and it normally occurs between Spring and Autumn, when the land becomes warmer than the adjacent ocean. Its formation is favored when the synoptic conditions allow strong heating in the land areas, giving to at least a land-sea temperature difference of (3 – 6) ºC. The development and location of the convection is influenced by the sea breeze, which it is influenced by the wind conditions prevailing in the area. The convection is favored under potentially unstable atmospheric conditions, thus the choice of an atmospheric sounding with an unstable temperature profile is crucial to characterize the ideal initial atmosphere. The differential heating created by the solar irradiance during the daytime gives place to a surface pressure gradient, which generates wind associated with the thermal circulation, in order to homogenize the pressure field.

An estimate of the strength of the sea breeze can be obtained by introducing: (1) the mathematical term of circulation as the integral line around a close curve of the velocity field and, (2) the Kelvin's circulation theorem for a baroclinic fluid where the isopycnic and isobar surfaces are not parallels.

CIRCULATION → $C = \oint v \, dl$ (1)

where v is the horizontal component of the wind vector.

KELVIN'S THEOREM OF CIRCULATION $d_t C = \dfrac{\oint dP}{\rho} = \oint RT \, dln(P)$ (2)

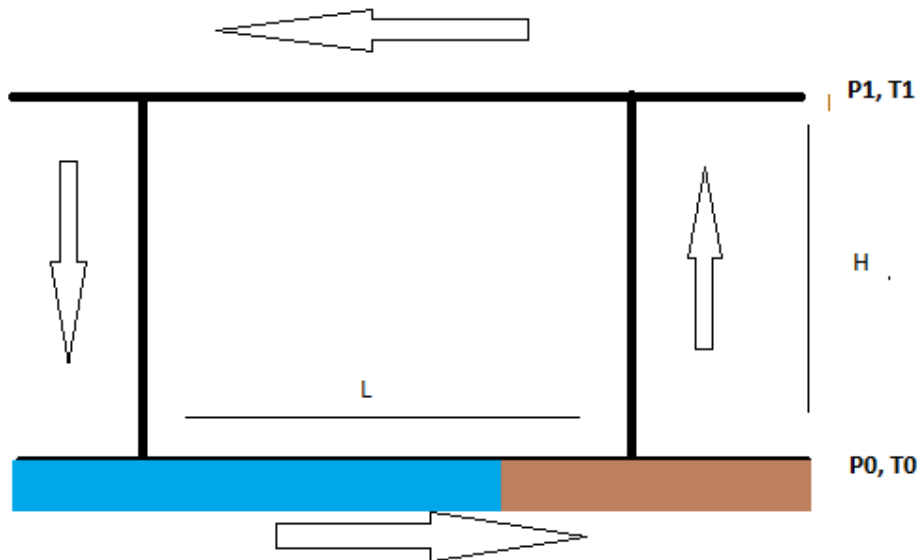where T is the temperature, R is the Universal Gas Constant and P is the pressure.

Figure 2: Vertical section of the thermal circulation during daytime. Where P0,T0 are the pressure and the temperature at the surface, and P1 and T1 are the pressure and the temperature at the level located at the distance H in the vertical. L is the horizontal distance that reaches the circulation.

First, the total temporal variation of the circulation is equal to integrate the solenoidal term along the curve.

$$d_t C = \oint_{P_0}^{P_1} RT \, dln(P) + \oint_{P_1}^{P_1} RT \, dln(P) + \oint_{P_1}^{P_0} RT \, dln(P) + \oint_{P_0}^{P_0} RT \, dln(P) = R(T_0 - T_1) \ln\left(\frac{P_0}{P_1}\right)$$

And, on the other hand: $d_t C = \oint d_t v\, dl + \oint v\, d_t l = \oint d_t v\, dl$

Where: $d_t v = \dfrac{d_t C}{2(H+L)}$ Then: $d_t v = \dfrac{R(T_0 - T_1)\ln\left(\dfrac{P_0}{P_1}\right)}{2(H+L)}$

An approximation of the hight that the thermal circulation could attain (H), which it is necessary before obtaining the acceleration of the wind. Taking into account mean values that can take place around the mean sea level: Surface pressure ($P_0 = 1000$ hPa), upper pressure ($P_1 = 900$ hPa),　mean surface temperature ($T_{med} = 288$ k), gravity ($g = 9.81$ m/s²), Universal Constant for dry air (R = 287 J/ Kg K), horizontal length (L = 50000 m) and thermal difference between land and sea ($T_0 - T_1 = 4$ k). And using the hypsometric equation, the value of the circulation's height is obtained:

$$H = \frac{R\,T_{med}\,\ln\left(\dfrac{P_0}{P_1}\right)}{g} = 888\,m$$

Therefore, the acceleration will be:

$$d_t v = \frac{R(T_0 - T_1)\ln\left(\dfrac{P_0}{P_1}\right)}{2(H+L)} = 1.298 * 10^{-4}\ \frac{m}{s^2}$$

Once the acceleration is known, we can calculate the wind speed after a time of two hours.

$$v(t = 2h) = v_t\, t = 9.05\,\frac{m}{s} = 32.6\,\frac{km}{h} = 17.6\,kt$$

As time goes by, the wind speed increases until isolation reaches its maximum. Surface winds between 10 and 20 knots are common through a vertical deep of about 150 meters

while the entire breeze circulation could reach between 450 and 900 meters hight over the surface.

To this result, the dependency with the synoptic mean flow has to be added in order to obtain the modulus and direction of the resulting velocity vector, in principle as a vectorial sum of wind field generated from the sea breeze and the synoptic wind field. It is an approximation due to the non-linear interactions between both fluxes.

The sea breeze can interact with other surface features such as outflow boundaries, convergence lines or even other sea breeze fronts leading to the development of convection. In the interaction between two ore more see breeze fronts, there is a supply of moisture by advection coupled with the convergence of winds, a factor that serves as trigger mechanism for the development of cumulunimbus under unstable synoptic conditions.

4 CONVERGENCE ZONES

It is worth to analyze the origin of the convergence areas in order to have a better interpretation of the wind field generated by the sea breeze over the domain of study for every simulation.

The convergence is a low level mechanism for the development of convection. From the mathematical point of view, it can be analyzed in terms of the tangential acceleration and the confluence of the wind field being the condition for convergence $\nabla V < 0$

The next equation shows the convergence in the intrinsic coordinate system where "s" and "n" are the tangential and normal component respectively:

$$\nabla V = \partial_s V + V \partial_n \Theta$$

Term of tangential acceleration:

$\partial_s V < 0$ is obtained when there is a slowdown in the wind speed along the streamlines.

Term of confluence:

$V \partial_n \Theta < 0$ the streamlines converge to a point

In order to study the combination of terms mathematically in terms of the cartesian coordinate system, the convergence can be related with the log temporal variation of the area occupied by the fluid.

wind speed components: $u = d_t x$ and $v = d_t y$

$$\nabla V = \frac{\partial \, dy}{\partial_x dy} \frac{dx}{dt} + \frac{\partial \, dx}{\partial_y dx} \frac{dy}{dt} = \frac{1}{A} d_t A \quad So, the\, condition\, of\, convergence\, is: \quad \frac{1}{A} d_t A < 0$$

METHODOLOGY

1 MM5 Numerical Model

1.1 Introduction to MM5

MM5 numerical model was developed by the University of Pennsylvania State and the National Center and the National Center for Atmospheric Research of the United States (NCAR). It is a non-hydrostatic model which allows us to solve mesoscale processes with a horizontal resolution of a few kilometers. It has the capability of multiple-nest and four dimensional data assimilation; and it can be initialized with different sources of analysis of global atmospheric models such as the Global Forecast System (GFS) run by NOAA, or the Integrated Forecast System (IFS) run by European Centre for Medium-Range Forecasts (ECMWF). It also can be initialized with observations from weather stations and soundings.

1.2 Non-hydrostatic dynamics

Once the horizontal scale of the simulated phenomena becomes shorter than the vertical scale, non-hydrostatic process must be taken into account. For structures with a scale smaller than about 10 km, the meteorological numerical model has to incorporate non hydrostatic processes to resolve its dynamical core implemented.

In a hydrostatic process, there is an equilibrium between the vertical pressure gradient and gravity, so the pressure is determined by the air conditions in the layers above. On the contrary, for the non hydrostatic dynamics, there can be an explicit vertical acceleration because there is not an equilibrium between these two forces. Pressure perturbation from a reference state together with the vertical momentum, become two extra predicted variables that have to be initialized. This non-hydrostatic balance allow us to solve the vertical

acceleration that occurs on mesoscale phenomena such as convection under sea breeze conditions.

1.3 The MM5 model vertical and horizontal grid

The vertical coordinate used by MM5 is σ, the low levels follow the terrain while the upper levels are flat. It ensures that the ground match the lower sigma surface, preventing the surface from intersecting with the orography, as it occurs when it is taken as a vertical coordinate the geometric height, pressure or potential temperature. Nevertheless, the strong influence of the topography on the sigma levels, could cause problems in the calculation of horizontal pressure gradients. All the equations governing the dynamics of the model have to be rewritten in the sigma coordinate:

$$\sigma = \frac{p - p_t}{p_s - p_t}$$

Where σ is zero at the top and one at the surface. The resolution of the boundary layer is higher than in the upper levels, an obvious advantage to better resolve the boundary layer processes. Note also in Fig.3, the staggering of different model variables in the vertical.
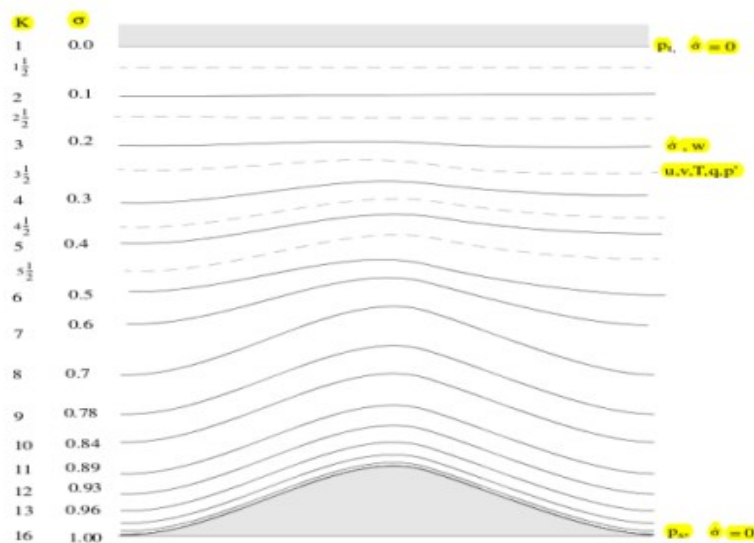
Figure 3. Schematic representation of the vertical structure of the model. Dashed lines denotes half-sigma levels, solid lines denote full-sigma levels.

The horizontal grid points follow an Arakawa-Lamb B-staggering where the scalar variables as the temperature, specific humidity, etc are located in the center of the grid square and the zonal and meridional components of the velocity are located in the corner of every grid square. Although in this case of study only one domain has been chosen, it is possible to run several domains at the same time nesting them with "two ways interaction" or "one way interaction", see (Fig.4).
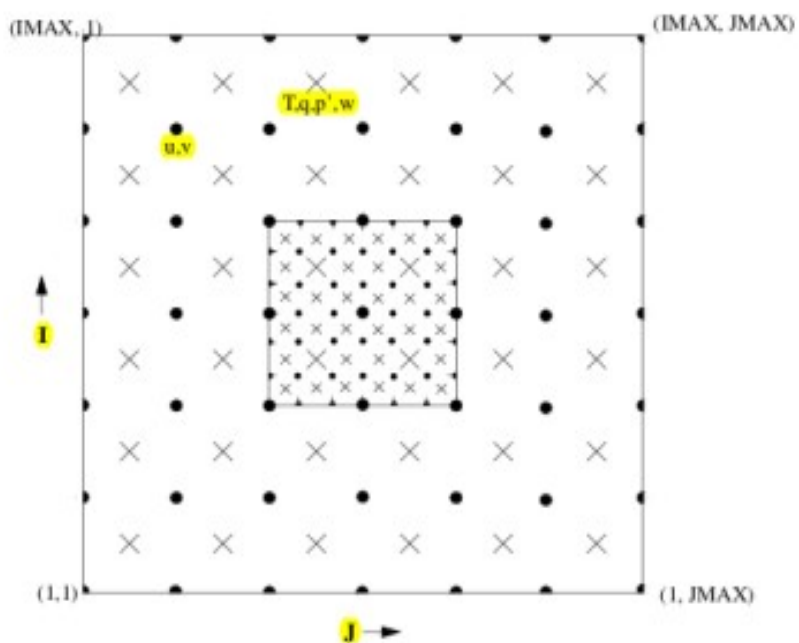
Figure 4. Schematic representation of the Arakawa-Lamb B-staggering.

1.4 Lateral Boundary Conditions

As any regional model, MM5 requires lateral boundary conditions. All the four lateral boundaries have specified wind, pressure, temperature, moisture field, and can have specified microphysical fields. A large-scale analysis is normally used in order to specified these variables at the outer row and column but it is important to know that in the next four rows and columns from the border, the model is nudged towards the analyses, and there is also a smoothing term. During the simulation strong gradients could be generated structures and they do not spread throughout the domain thanks to the smoothing term. For our experiments, the lateral boundary conditions differ in the horizontal wind components for each simulation, conditions that remains invariant during the course of the simulation.

1.5 Land-Use Categories

With regard to the land-use, several surface properties such as albedo, roughness length, long wave emissivity, heat capacity and moisture availability are assigned to every grid point. All these surface properties follow climatological values that depend on the season. The differential heating between land and sea depends on the amount of short-wave radiation arriving from the sun, but it also depends on surface properties considered by the model as the heat capacity, which depends on the moisture availability. It is in summer when the conditions are appropriate to reach the thermal gradient necessary for the sea breeze formation.

1.6 Data required to run MM5

In short, the required data to run the model are:

- Topography and land use.

- Gridded atmospheric data that have at least these variables: sea-level pressure, wind, temperature, relative humidity, geopotential height, and at least these pressure levels: surface, 1000, 850, 700, 500, 400, 300, 250, 150 and 100 mb. The temperature, wind and relative humidity is taken from the atmospheric sounding.

- Optional: observational data from soundings and surface reports.

1.7 MM5 Modules

TERRAIN: The following characteristics of the domain are configured: the position of the center of the domain, the resolution (distance between two grid points) and the horizontal extension of the domain (number of grid points). The aim of this module is to interpolate the regular latitude-longitude surface terrain elevation and the land use within the chosen domain and resolution. Moreover, multiple nested domains can be configured.

REGRID: the archived gridded meteorological analyses data is interpolated into the domain resolution established in the previous module. Two dimensional interpolation is performed on the pressure levels and the surface analyses.

RAWINS: This module allows us to introduce real surface and upper-air observations in order to improve the initial conditions of our simulation.

INTERPF: The purpose of this module is to interpolate all analyses data from pressure to sigma levels. This is because the physical and dynamical equations of the model uses σ as a vertical coordinate.

MM5: Convective systems are meso-beta and meso-gamma scales (2 to 200 km) and can be successfully simulated by the MM5 model. The prognostic equations are integrated in this module to determine the temporal evolution of the initial conditions that were established

in the previous modules. Apart from the dynamical equations, this model offers a variety of parametrizations from low to hight computational cost, which are able to resolve the subgrid scale physical processes: parametrization of clouds, microphysics, boundary layer and radiation. The time step has to be defined according to the Courant-Friedrichts-Lewy (CFL) condition, which is a necessary condition for computational convergence when solving partial differential hyperbolic equations by the method of finite differences.

INTERPB: The MM5 output has to be understandable to the data processor vis5d. Therefore, the aim of this model is to interpolate back the output from σ to pressure levels. The output is suitable for input to REGRID in the case of re-grid a model forecast.

Most of our post-analysis is performed with vis5d, which is a diagnostic and visualization tool applied on pressure levels.

2 Verification Method

The verification process is essential for the Numerical Weather Prediction (NWP). There are some quality measures in terms of scores based on grid points errors adapted to synoptic-scale. However, these are not appropriate for complex structures like precipitation and thus, our verification would not be judged fairly, Wernli et al. (2008). The location or timing error in the forecast are penalized double. Forecast rain where there is not observed rain (or the opposite case) lead to "double penalty" and this problem is proportional to the resolution of the models, thus it could give better scores to a coarser grid model. Traditional indices also do not correlate patterns or structures so objects like rain cells are not captured by point-to-point verification. Among all of these quality measures based on grid points error are the classical methods for continuous variables like Bias, Root Mean Square (RMS), Mean Absolute Error (MAE), and Anomaly Correlation Coefficient (ACC). On the other hand, there are classical methods based in categorical variables. Particularly, the quality of Quantitative Precipitation Forecast (QPF) is assessed using categorical information in Jolliffe and Stephenson (2003).

Table 3.1 The four possible outcomes for categorical forecasts of a binary event

Event forecast	Event observed	
	Yes	No
Yes	Hit	False alarm
No	Miss	Correct rejection

Table 1. The events are classified in a box attending by if they were or not observed and predicted. Jollife and Stephenson, (2003).

2.1 Object oriented method

Once that the shortcomings of the classical methods based in grid points errors have been explained, a variety of object oriented methods were developed in order to avoid the double penalty problem:

- The CRA (entity-based) verification (Ebert and McBride, 2000) was created in order to answer what is the location error of the spatial forecast and how does the total error break down into components taking into account the incorrect location, volume, and fine scale structure. This was a pioneering study, the total mean squared error was decomposed into components associated with the location, rain volume, and pattern of identified precipitation objects.

- Method for Object-based Diagnostic Evaluation (MODE) (Brown et al.,2004 ; Davis et al., 2006) focuses in the similarities of the forecast objects compared to the observed objects according to a variety of descriptive criteria.

- Event verification using composites (Nachamkin, 2004).

- Cluster analysis (Marzban and Sandgathe, 2008).

- Procrustes shape analysis (Michaes et al., 2007; Lack et al., 2010).

- Structure- Amplitude-Location (SAL) (Wernli et al., 2008).

2.1.1 Structure-Amplitude-Location (SAL)

This is a scientific method based on objects and "fuzzy" verification techniques that requires that the forecast and the observations are in approximate agreement in time, space and intensity. Specifically, it has three scores related with three different aspects of the structure (S), amplitude (A), and location (L), and it makes a judgment closer to a subjective visual interpretation. These scores, in addition to avoid the double penalty in our verification tasks, allow us to condense and quantify much information in these three scalar scores.

First of all, an identification of objects has to be made for every precipitation field, denoted as R, in order to identify coherent objects which are necessary for the obtention of the structure and location components. This process does not require a one-to-one matching between the identified objects in the observed precipitation field and the forecast precipitation field.

Wernli and Sprenger, (2007) has developed an algorithm in order to identify every grid point which belongs to an object of precipitation. From now on, a threshold value is calculated from the maximum of precipitation R_{max} that occurs within the domain D. The election of the factor "f" is a critical point which it is not based on objective criteria by Wernli *et al* , (2008).

A factor equal to 1/15 was established in their work owing to the fact that in most of the considered cases the precipitation contour separates features reasonably. The Meteorological Institute of the University of Bonn has been working with these scores using as a threshold the 95%-percentile of the precipitation field or using different thresholds (0.1, 1, 2 and 5 mm/h) in order to explore if the SAL measures vary with the thresholds. They conclude that the thresholds are non-unique for different weather cases, confirm the selection of the threshold as a critical factor.

Taking this into account, every object will be constituted of neighboring grid points as long as the precipitation's grid points R_{ij} will show larger values than R', where:

$$R' = f R^{max} \quad (1) \quad .$$

The amplitude component (A)

This component is the normalized difference between the domain-averaged precipitation of the forecast minus the domain-averaged precipitation of the observations. This score is in relation with the total amount of precipitation.

$$A = \frac{D(R_{for}) - D(R_{obs})}{0.5[D(R_{for}) + D(R_{obs})]} \quad (2)$$

where D(R) denotes the domain average of R:

$$D(R) = \frac{1}{N} \sum_{(i,j) \in D} R_{ij} \quad (3)$$

Thus, it means that the threshold chosen does not affect to this score, it takes into account all the grid points even if its precipitation is less than the threshold, $R_{ij} < R'$, see Eqt. (1).

To summarize, it quantifies the accuracy of the amount of precipitation of our simulations independently of the spatial structure. A presents values within the range [-2, 2].

- A = 0 means perfect forecast.
- A > 0, the model overestimates, where A = 1 indicates that our model overestimates the precipitation domain-averaged in a factor 3.
- A < 0 model underestimates, where A = -1 means that our model underestimates the precipitation domain-averaged by a factor 3.

The location component (L)

This index is composed by two components L_1 and L_2. They take care of the precipitation distribution. The first component of the index L_1 is the normalized distance between the center of mass of the modeled and observed precipitation fields, giving a first order indication of the accuracy of the precipitation distribution:

$$L_1 = \frac{\left| x\left(R_{for}\right) - x\left(R_{obs}\right)\right|}{d} \quad (4)$$

Where d is the largest distance between two boundary points of the considered domain $\mathcal{D}$ and x(R) is the center of mass of the precipitation field within the domain $\mathcal{D}$. Due to the fact that L_1 has been normalized, its values oscillate within the range [0, +1] . L = 0 indicates that the center of mass of both fields are localized at the same position, but we should bear in mind that two different precipitation fields can have L = 0, and it does not mean that this situation is a perfect forecast. The figure 5 shows the case of the modeled and observed precipitation field, but L_1 is rotation invariant, it means that an object around its center of mass does not change the score L_1.
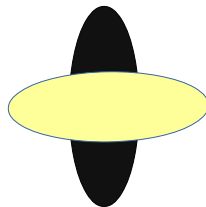
Figure 5. Simple scheme of one object modeled in black and one observed in yellow, where L = L_1, in this particular case L = L_1 = 0, due to the fact that the center of mass of both fields match.

In order to distinguish such situation, the second part of the index L_2 considers the average distant between the center of mass of the total precipitation field with every individual precipitation objects. L_2 is also rotation invariant, rotating the whole field does not change L_2.

An integrated amount of precipitation is calculated for every object as follows:

$$R_n = \sum_{(i,j) \in R_n} R_{ij} \quad (5)$$

- R_n extends only if $R_{ij} > R'$, see Eqt. (1). Thus, it only takes into account the grid points with precipitation exceeding the threshold.

The weighted average (5) distance between the center of mass of the individual objects X_n, and the center of mass of the total precipitation field, X, is given by the next expression:

$$r = \frac{\sum_{n=1}^{M} R_n |x - x_n|}{\sum_{n=1}^{M} R_n} \quad (6)$$

-r reaches the maximum value of d/2 what it means half of the maximum distance between two grid points in the Domain. In the case of a single object in the modeled and observed domain, r =0 owing to $X_n = X$.

With all these concepts, L_2 is obtained with the expression that relates the difference between the weighted average distance obtained above for the forecast and observed fields. We should not forget that in this calculations only $R_{ij} < R'$ have been taken into account:

$$L_2 = 2 \frac{|r(R_{for}) - r(R_{obs})|}{d} \quad (7)$$

L_2 takes values that range between [0,1]. Therefore, the total location component $L = L_1 + L_2$ range between [0,2]. The weakness of the definition of L is that it is not sensitive to rotation around the center of mass, as it was demonstrated for L_1 and L_2.

The structure component (S)

This score is related with the shape and size, which aim is to compare the normalized precipitation objects Vn, defined with the next expression:

$$V_n = \frac{\sum_{(i,j) \in R_n} R_n}{R_n^{max}} \quad (8)$$

R_n^{max} is the maximum precipitation value within the object, where: $R_n^{max} \leqslant R^{max}$

This scale precipitation volume is calculated for all the objects, making this scale necessary in order to differentiate it from the amplitude score A. Then, a weighted mean for all the objects scaled precipitation volume is calculated with the next expression for both datasets, forecast and observed fields.

$$V(R) = \frac{\sum_{n=1}^{M} R_n V_n}{\sum_{n=1}^{M} R_n} \quad (9)$$

where V(R) is proportional to the second moment of the precipitation field R_n^2.

Bearing in mind these concepts, S is defined as a normalized difference in V, with the same criteria used for the component A:

$$S = \frac{V(R_{for}) - V(R_{obs})}{0.5[V(R_{for}) + V(R_{obs})]} \quad (10)$$

- S takes values between the range [-2,2].

- $S > 0 \rightarrow$ model predicts widespread precipitation events compared to the observations.

- $S < 0 \rightarrow$ model predicts peaked or more convective precipitation events compared to observations events.

All the scores have to be taken into account in order to perform an accurate verification. The components S and A are strongly related.

For a deeper understanding of these scores, the reader is referred to the publication (Wernli et al., 2008).

3 DESCRIPTION OF THE PROJECT

All the simulations performed in this study have been automated with the MM5 regional model which was introduced in the previous section. The project is composed in two parts; on the first part, thirty-two simulations have been compared with a control simulation in order to verify how the synoptic wind field affects to the convergence of the sea breeze over the island of Majorca. On the second part, the thirty-two simulations have been run with the same initial and boundary conditions, but with the orography set in a constant value of one meter above the sea level, with the aim of identifying the influence of the orography on the convergence. The basis of this project is supported by initial idealized atmospheres. The scheme of the Fig. 6 shows schematically the steps for the development of the simulations in an MM5 context.
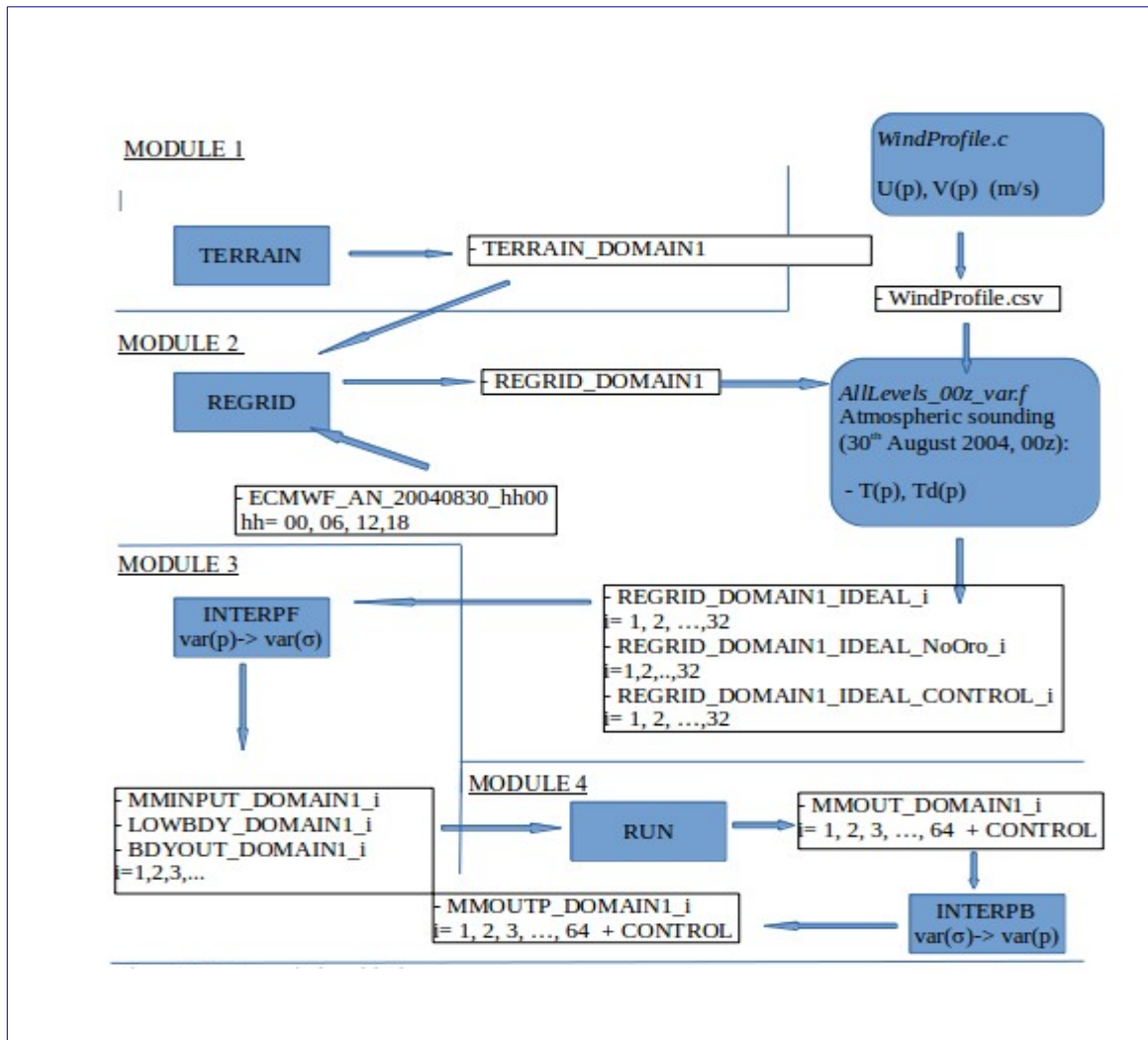
Figure 6. MM5 numerical model scheme.

3. 1 Definition of the domain of study

All the configurations are set in the module (1) according the scheme of Figure 7, the aim is to define the domain of study in which all the simulations are performed. The following features have been established: A single domain has been processed, which is center at the latitude $\varphi = 39.6^{\circ}$ and longitude $\lambda = 2.9^{\circ}E$ (located at the center of the island of Majorca). The horizontal extension of the domain is 196x196 grid points with a resolution of

1km, which is enough to cover the whole island of Majorca. This horizontal resolution is based in a Lambert Conformal projection which preserves the angle between two points measured in the reference Earth surface and in the map.

The initial conditions are defined in eleven vertical pressure levels (1000, 950, 900, 800, 750, 650, 600, 550, 450, 350) hPa which there were converted to the vertical resolution set in the model, with 31 σ levels. It is due to the fact that the equations of the model are based in this vertical coordinate.

The forecast time is 24 hours starting at 00 UTC on 30th August 2004 and finishing at 00 UTC on 31th August 2004. The time step is 4 seconds respecting the Courant-Friederich-Lewy (CFL) condition.

3.2 Definition of the initial and boundary conditions for every scenario

The initial and boundary conditions for the control simulation, and for the rest of the thirty-two simulations have been created in the module (2) of Fig. 6. All the scenarios have in common the temperature and dew point vertical profiles, which have been established from the atmospheric sounding launched from Son Bonet, Majorca at 00z on 30th August 2004, while the zonal and meridional wind vertical profiles are different for each scenario.

3.2.1 Atmospheric sounding

This atmospheric sounding at 00z on the 30th 2004 has been chosen due to the fact that convective precipitation was detected on that day, being the sea breeze the triggering mechanism. The temperature and the dew point vertical profiles are represented in a Skew-T diagram on the left hand size of Figure 8, where the proximity of both curves at low levels

indicates that, there is moisture available. On the right hand side, the vertical wind intensity and direction is plotted. A turbulence area is founded near to 850 hPa, due to the wind shear in those levels caused by the variation in the intensity and direction of the vertical wind. The wind shear is favorable to the organization of the convective system. The single isotherm layer located above 200 hPa indicates that the tropopause is placed at that level.

Under the context of sea breeze conditions, there will be a continuous advection of moisture through the main inflows of the sea breeze along the Bays of *Palma* and *Alcudia*. This supply of moisture is essential for the development of the deep convective clouds, with a greater amount of precipitation.
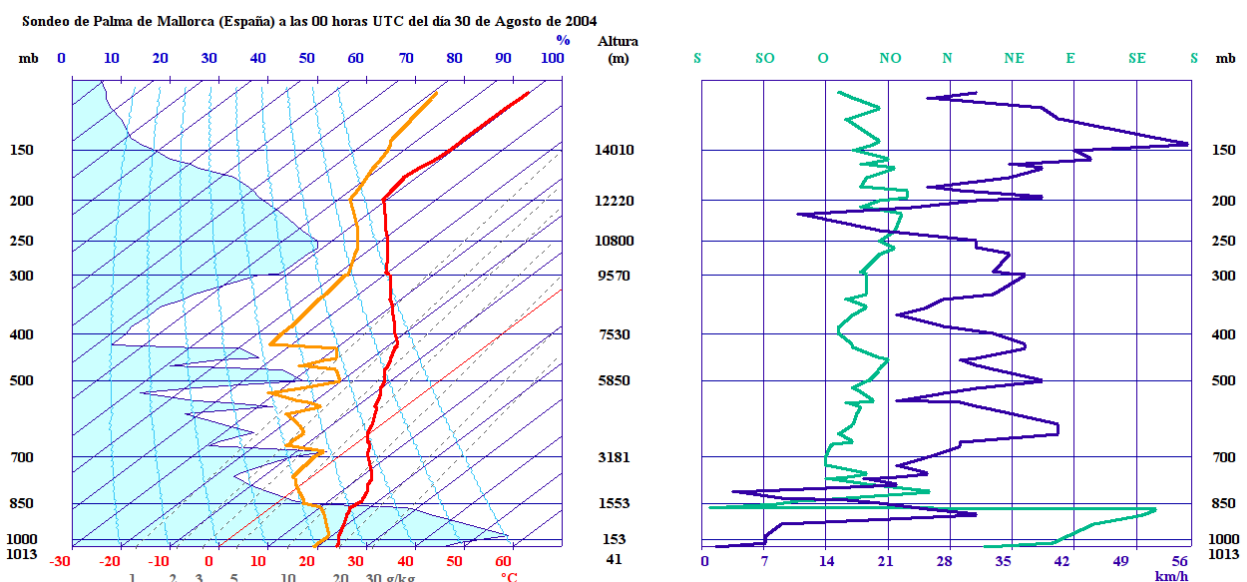
Figure 7: Plot of the atmospheric sounding launched at 00 UTC, 30th August 2004, in Son Bonet (Majorca). On the left, the temperature and dew point vertical profiles are represented in a thermodynamic diagram Skew-T. On the right, the module and direction of the wind are represented along the vertical.

Station information and sounding thermodynamic indices:

The atmospheric sounding was launched from the weather station located in Son Bonet, near to the Bay of Palma, which has a latitude of 39.61º and a longitude of 2.71ºE. The weather station has an elevation of 41 meters above the sea level.

The Convective Available Potential Energy (CAPE) is the available energy to lift an air mass by buoyancy. It is represented by the area enclosed in the diagram by the environmental temperature profile and the pseudo-adiabatic followed by the surface parcel, running from the Level of Free Convection (LFC) at 727.49 hPa to the Equilibrium Level (EL) at 194.01 hPa. In this particular case, the high values of CAPE with 1242.06 J/kg, shows greater potential for strong convection. The convective inhibition (CIN) indicates the amount of energy that will prevent the surface air parcel to reach the (LFC), it is represented by the area enclosed by the environmental temperature profile and the temperature of the parcel lifted from some originating level to the (LFC). The higher is the (CIN) value, the lower the likelihood of convective convection. In this case, the (CIN) value of -105.53 J/Kg indicates that not much energy is required to lift the parcel to the (LFC); this is explained by the high values of moisture at the low levels.

Attending to the stability scores, the Liftex Index (LI) is calculated as the difference between the observed temperature at 500 hPa and the temperature of an air parcel lifted 500 hPa from the near surface. The value of LI equal to -3.91 shows a moderate unstable environment, because the air parcel lifted reaches the level of 500 hPa with a temperature 3.91 ºC higher than the environment. The Showalter Stability Index (SSI) is similar to the (LI), but it uses a parcel lifted from 850 hPa to 500 hPa, the SSI has a value of 3.17 showing an environment less unstable than the LI, due to the fact that it under-represents the instability caused by the moist layer located below 850 hPa.

The Total Totals Index (TT) is calculated using the temperature and dew point at 850 hPa and the temperature at 500 hPa. The higher the 850 hPa temperature and dew point, and the lower the 500hPa temperature, the greater instability and the resulting TT value. The TT in this atmospheric sounding indicates moderate instability with a value of 44.4.

The K Index takes into account the vertical distribution of both moisture and temperature, it is obtained from the temperatures at 850, 700 and 500 hPa, and dew points at 850 and 700 hPa. In this case, the value of K equal to 22.3 shows also moderate instability.

The Severe Weather Threat (SWEAT) index differs from many of the other indices analyzed so far, in that it takes into account the wind profile, which also affects to instability. The inputs of this index include: the TT index, the dew point at 850 hPa, and the wind speed and direction at 850 and 500 hPa. The value of 110.19 from out atmospheric sounding shows low potential for severe thunderstorms.

The Bulk Richardson Number (BRN) is the ratio between the convective available potential energy and the vertical wind shear. The value obtained of 68.84 shows a (CAPE) much higher than the wind shear, thus single cell storms are favored in such situation.

CAPE (J/Kg)	CIN (J/Kg)	LI	SSI	TT	K	SWEAT	BRN
1242.06	-105.53	-3.91	3.17	44.4	22.3	110.19	68.84

Table 2. Summary of the static stability indices and thermodynamic parameters.

3.3 The control simulation:

Obtaining a simulation as a reference, a control simulation was first defined canceling the initial and boundaries conditions of the horizontal wind profiles along the vertical at the low levels, from the surface to 700 hPa. But the wind field obtained was influenced by the exchange of momentum from the upper levels to the surface during the simulation, thus, the sea breeze could not be isolated from the synoptic wind field. Then, our control simulation was finally defined with an atmosphere initially at rest at all vertical levels (a condition maintained also for the boundary forcing) in order to fully isolate the sea breeze formation and evolution. This simulation takes into account the complex orography of Majorca, which influences the wind field generated by the thermal differences.

3.4 The thirty two initial idealized atmospheres:

As the first part of this project, thirty-two scenarios with different wind profiles as initial and boundary conditions have been simulated. The aim is to assess how the synoptic wind field affects to the sea breeze convergence, under conditions of instability. Eight possible directions have been chosen (N, NE, E, SE, S, SW, W, NW), because the impact of the synoptic wind will be different, due the complexity of the orography of Majorca. Four possible wind intensities have been simulated for each direction, the convergence of the sea breeze will be weakly affected for low wind intensities, but the convergence will be inhibited for the cases with higher intensity. There are other triggering mechanisms as the orography, that can lead to convection under instability conditions provided by the vertical profile of temperature and moisture in the atmospheric sounding.

The orography not only interacts with the synoptic wind field, it also exchanges momentum with the wind patterns generated by thermal differences. The mountains and associated valleys play an important role in the evolution of the sea breeze, the contribution of them could even lead to early sea breeze development, due to its connection with the circulation of the mountains-valleys. The complex orography of Majorca tends to determine the distribution of heating and the locations into which the sea breeze front can penetrate. These conditions make that the main sea breezes fronts in Majorca take place in certain areas such as the Bay of *Palma*, located in the south-west or the Bay of *Alcudia*, situated in the north-east.

As the second part of this project, the initial idealized scenarios with the same initial conditions have been run again, but this time, the orography of the whole island of Majorca has a constant value of one meter above the sea level, for all the simulations (in practical terms, the orography is eliminated). If the relief is not taken into account, the sea breeze fronts will come through all its shores producing strong convergences within the island, where a bigger amount of precipitation is expected. As the intensity of the synoptic wind field in the initial and boundary conditions increases, it is expected to have a greater influence on

the convergence of the sea breeze fronts, since the general wind will not find topographic obstacles in its path.

The initial and boundary idealized conditions for the horizontal wind profile are as follows:

45º	$U(p) = -2,5$ m/s $V(p) = -2.5$ m/s	90º	$U(p) = -3.536$ m/s $V(p) = 0$ m/s
	$U(p) = -5$ m/s $V(p) = -5$ m/s		$U(p) = -7.071$ m/s $V(p) = 0$ m/s
	$U(p) = -7.5$ m/s $V(p) = -7.5$ m/s		$U(p) = -10.607$ m/s $V(p) = 0$ m/s
	$U(p) = -10$ m/s $V(p) = -10$ m/s		$U(p) = -14.142$ m/s $V(p) = 0$ m/s
135º	$U(p) = -2,5$ m/s $V(p) = 2.5$ m/s	180º	$U(p) = 0$ m/s $V(p) = 3.536$ m/s
	$U(p) = -5$ m/s $V(p) = 5$ m/s		$U(p) = 0$ m/s $V(p) = 7.071$ m/s
	$U(p) = -7.5$ m/s $V(p) = 7.5$ m/s		$U(p) = 0$ m/s $V(p) = 10.607$ m/s
	$U(p) = -10$ m/s $V(p) = 10$ m/s		$U(p) = 0$ m/s $V(p) = 14.142$ m/s
225º	$U(p) = 2,5$ m/s $V(p) = 2.5$ m/s	270º	$U(p) = 3.536$ m/s $V(p) = 0$ m/s
	$U(p) = 5$ m/s $V(p) = 5$ m/s		$U(p) = 7.071$ m/s $V(p) = 0$ m/s
	$U(p) = 7.5$ m/s $V(p) = 7.5$ m/s		$U(p) = 10.607$ m/s $V(p) = 0$ m/s
	$U(p) = 10$ m/s $V(p) = 10$ m/s		$U(p) = 14.142$ m/s $V(p) = 0$ m/s
315º	$U(p) = 2,5$ m/s $V(p) = -2.5$ m/s	360º	$U(p) = 0$ m/s $V(p) = 3.536$ m/s
	$U(p) = 5$ m/s $V(p) = -5$ m/s		$U(p) = 0$ m/s $V(p) = 7.071$ m/s
	$U(p) = 7.5$ m/s $V(p) = -7.5$ m/s		$U(p) = 0$ m/s $V(p) = 10.607$ m/s
	$U(p) = 10$ m/s $V(p) = -10$ m/s		$U(p) = 0$ m/s $V(p) = 14.142$ m/s

Figure 8. Initial and boundary conditions of the horizontal wind for the thirty-two simulations with orography and the thirty-two simulations with non-orography.

The aim of the last part of this dissertation is to apply the oriented object method SAL in order to quantify the differences between the simulation with orography and its counterpart with the constant orography of one meter above the seal level. This method of verification is applied for thirty-two different scenarios.

3.5 Interpolation of the initials and boundary conditions from vertical pressure levels to vertical σ levels

The last step is to get the initial, the bottom and the lateral boundaries conditions over the vertical σ levels in order to get the input data ready for every simulation, module (4) of Fig. 6. Since every simulation has a high horizontal resolution of 1 km, the number of computational levels has been interpolated from 11 pressure levels to 31 σ levels, providing a higher vertical resolution, which is important for the mesoscale processes as the development of sea breeze fronts. The fact that the MM5 model is a non-hydrostical allows to calculate the vertical accelerations in each σ level, hence it is appropriate to have a higher vertical resolution at low levels due to the sea breeze is basically a boundary layer phenomenon.

$$\sigma(31) : U(\sigma(31)), V(\sigma(31)), T(\sigma(31)), Td(\sigma(31))$$
$$\sigma(30): U(\sigma(30)), V(\sigma(30)), T(\sigma(30)), Td(\sigma(30))$$
$$\sigma(2) : U(\sigma(2)), V(\sigma(2)), T(\sigma(2)), Td(\sigma(2))$$
$$\sigma(1) : U(\sigma(1)), V(\sigma(1)), T(\sigma(1)), Td(\sigma(1))$$
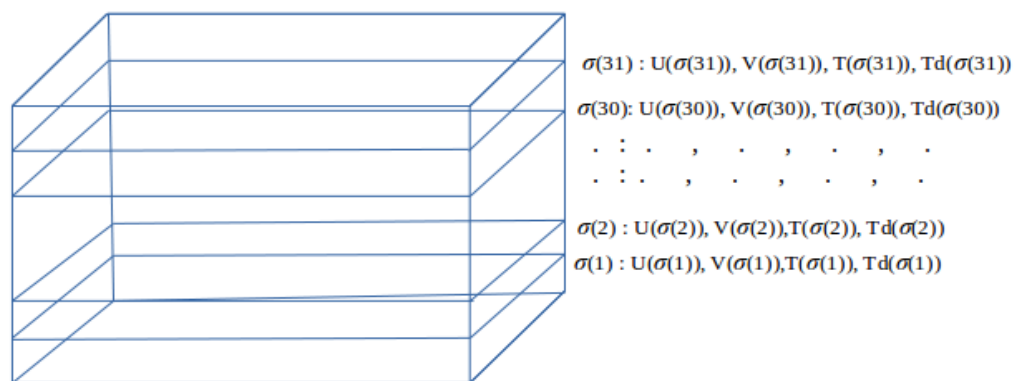
Figure 9. Vertical profiles of the initial and boundary conditions in σ levels.

4 Simulation products

Once the idealized atmosphere has been created for each scenario, the instability implicit in the vertical conditions of temperature and moisture might be released in the form of convection if triggering mechanisms of different origins are properly simulated. The vertical temperature profile will become more unstable at low levels, as the thermal radiation increases, what means that the parcel of air is heated enough from below, rising adiabatically until it is just saturated, reaching the Convective Condensation Level (CCL). But the dynamics occurring during the simulation is more complex, the circulations developed in the interior of the island by thermal differences between the sea and the land, provide low-level moisture and thus, the (CCL) is displaced to a lower altitudes making that less heating is needed below the air mass to reach that level. This increase of moisture at low levels also affects to other levels as the Lifting Condensation Level (LCL), making easier the convection obtained from dynamic origins as the convergence of the sea breeze fronts or the orography forcing. All these and another factors give an idea of the complex dynamics that is generated from a thermodynamic and mechanical origin, but the situation might become even more complex if the different initial and boundary vertical profile conditions of the wind are taken into account for each scenario.

5 Data processing

In order to analyze the convective processes which take place during the simulation, the total precipitation field is calculated from the stratiform and convective accumulated precipitation field. The zonal and meridional wind speed components at the surface level are used with the aim of determining the convergence areas when the sea breeze is well established at 14 UTC. The precipitation founded near the limits of the domain, which is generated by the presence of strong gradients in the boundary conditions has been eliminated.

RESULTS

The atmosphere is a chaotic system in which all the processes involved in it have non-linear interactions. The initial and boundary conditions of temperature, dew point and wind speed have been established as uniform in all the horizontal layers of the domain, with the aim of isolating the interaction of the synoptic wind field with the inner regimes generated by the thermal differences between land and sea within the domain. It gives a barotropic character to the atmosphere as an initial condition, but as the simulation evolves, horizontal thermal gradients are created by modifying the dynamics within the domain. Furthermore, the dynamics generated are influenced by the complex orography of the island.

1.1 CONTROL SIMULATION
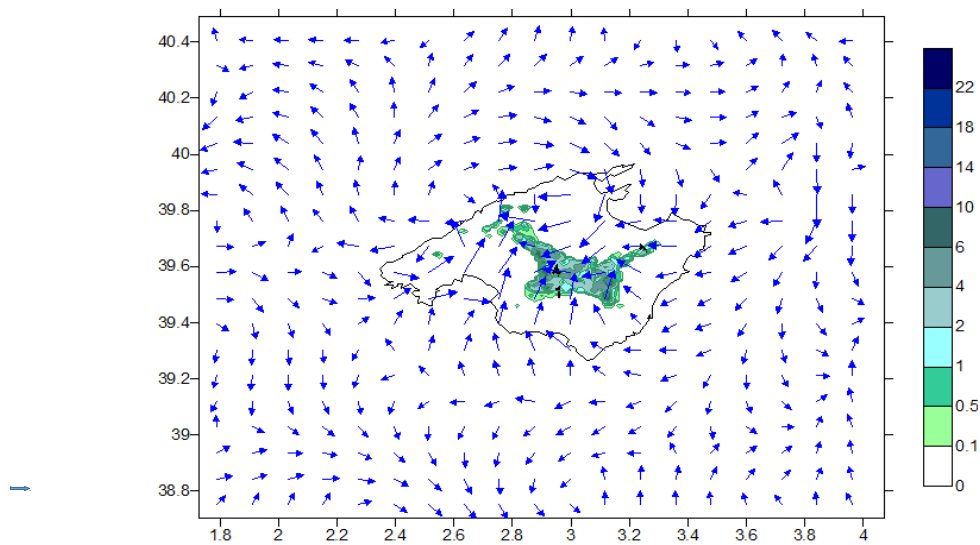
Figure 12. Control Simulation, the accumulated precipitation field (mm) with the wind field at 14 UTC. For the wind field, a vector length of 1 cm corresponds to 4.8 m/s.

The wind field depends exclusively on the differential heating between different land uses and the sea, since to the synoptic wind in this control simulation have been canceled in

the whole vertical. The mature sea breeze has been plotted in Fig. 12. There are two main inflows well defined along the Bay of *Palma* and the Bay of *Alcudia*, and a secondary inflow located in the southeast. The accumulative convective precipitation is a result of these three ingredients: the constant supply of moisture provided by the sea breeze, certain instability provided by the atmospheric sounding, and the enough intensity of the sea breeze in order to converge in the center of Majorca. The convergence of sea breezes supplies enough energy in order to raise a parcel of air up reaching the Level of Free Convection (LFC), and releasing the CAPE available in the environment. Fig.12 shows that the precipitation distribution is influenced by the orography. The precipitation field will be taken as a reference in order to apply the object-oriented SAL verification technique.

2 SIMULATIONS WITH OROGRAPHY

The simulation products obtained for the thirty-two different initial and boundary conditions have been presented according to the eight possible wind directions, in order to analyze how the areas of convergence is affected by the synoptic wind when the wind conditions increase, see annex. The comparisons of each scenario with the control simulation allow us to observe visually, and quantify the differences in the accumulated precipitation field, using the object-oriented SAL verification techniques. The component location (L), quantifies the displacement suffered by convective processes, as it measures the normalized displacement between the precipitation centers of mass. A second contribution L_2 has to be consider when there are more than one convective processes in the precipitation field, see Eqt. 7. The component Amplitude (A), takes into account the variation of the total precipitation with respect to the control simulation. For each direction, the variation of the precipitation as the wind intensity conditions are increasing, can be quantified attending to the evolution of (A). The component Structure (S) is more complex, but in the case that (A) keeps constant, a negative variation of (S) gives the idea, on the one hand that, the simulated precipitation is more peaked or convective with respect the control simulation. On the other hand, a positive

variation of (S) means that it is more homogeneous or stratiform in respect to the control simulation.

There is a threshold from which the synoptic wind is strong enough in order to displace the convergences out of the island and thus, there is not convective precipitation from this origin as a trigger mechanism. In these situations, the observed convective processes will be due to orographic forcing, due to the unstable conditions provided by the atmospheric sounding.

The SAL scores have been classified in four categories for the eight possible wind direction, attending to the initial wind conditions: WEAK → 7.5 m/s, WEAK-MODERATE → 7.1 m/s, MODERATE → 10.6 m/s and STRONG → 14.1 m/s.

2.1 DIRECTION 45º

Figures 1-4 of the Annex illustrate the comparative analysis between each scenario and the control simulation, and the accumulated precipitation field in twenty-four hours along with the horizontal surface wind field at 14 UTC.

WIND INTENSITY	WEAK	WEAK-MODERATE	MODERATE	STRONG
S	-0.48	-0.04	-1.42	-1.66
ΔS		0.44	-1.62	-0.24
A	-0.56	-0.39	-1.57	-1.61
ΔA		0.17	-1.18	-0.04
L	0.0064	0.0013	0.0999	0.1402

WIND INTENSITY	WEAK	WEAK-MODERATE	MODERATE	STRONG
ΔL		-0.0051	0.1000	0.0403
L1	0.0058	0.0001	0.0979	0.1374
L2	0.0006	0.0012	0.0019	0.0028

Table 1. Evolution of the scores Structure (S), Amplitude (A) and Location (L) for the initial and boundary wind directions of 45º.

Table 1 shows the scores obtained by the SAL technique for the wind direction set at 45º, as function of wind intensity. As the initial and boundary conditions of wind increase in intensity, the convective core decreases in the amount of precipitation. This is indicated by the gradual decrease in the score (A). There is an exception for the case with a weak-moderate wind intensity where there is a relative increase of precipitation. The evolution of the score (L) shows that distance between the center of mass of the precipitation fields is increasing, which means that the displacement of the convergence area towards the south-west increases as the synoptic wind intensity increases. The score (S) evolves in the same way as (A), marking a convective character for all the scenarios.

The relative increase in precipitation that occurs for the case of the weak-moderate wind intensity could be caused by the presence of Randa, with a height of 531 m. The convergence of the sea breezes could have an extra component due to the orographic forcing. The convection obtained for stronger initial wind is located outside the island.

In conclusion, it appears that convection under sea breeze conditions persists for cases of weak and weak-moderate wind conditions, but as the wind increases, the breeze from the Bay of *Alcudia* becomes stronger at the expense of the breeze from the Bay of *Palma* which weakens.

2.2 DIRECTION 90º

Figures 5-8 of the Annex illustrate the comparative analysis between each scenario and the control simulation, and the accumulated precipitation field in twenty-four hours along with the horizontal surface wind field at 14 UTC.

WIND INTENSITY	WEAK	WEAK-MODERATE	MODERATE	STRONG
S	-0.75	-1.76	-1.84	-1.32
ΔS		-1.01	-1.62	0.52
A	-0.67	-1.30	-1.86	-1.25
ΔA		-0.63	-0.56	0.61
L	0.0058	0.0914	0.1495	0.1135
ΔL		0.0856	0.1000	-0.0400
L1	0.0055	0.0891	0.1469	0.1107
L2	0.0008	0.0023	0.0026	0.0028

Table 2. Evolution of the scores Structure (S), Amplitude (A) and Location (L) for the initial and boundary wind directions of 90º.

Table 2 shows the scores obtained by the SAL technique for the wind direction set at 90º, as function of wind intensity. The easterly wind does not find much resistance throughout the Bay of *Alcudia,* leading to a rapid decrease in convection under sea breeze conditions. It is only the case of weak initial wind intensity, where the sea breeze developed in the Bay *of Palma* is strong enough in order to converge within the island. The amount of precipitation decreases and the main convective cell is displaced westwards.

For the stronger wind intensity, the convective cells are confined in the mountainous area of the *Serra de Tramuntana*, meaning that the convection appears under orographic forcing. The *Serra de Tramuntana* relief is oriented around 45º to the incident wind; therefore, the perpendicular component of the wind to the mountain range does not acquire high values. The evolution of the scores (A) and (S) are parallel showing a convective character of the precipitation for all cases.

2.3 DIRECTION 135º

Figures 9-12 of the Annex illustrate the comparative analysis between each scenario and the control simulation, and the accumulated precipitation field in twenty-four hours along with the horizontal surface wind field at 14 UTC.

WIND INTENSITY	WEAK	WEAK-MODERATE	MODERATE	STRONG
S	-0.90	-1.90	-1.13	-0.91
ΔS		-1	0.77	0.22
A	-1.00	-1.84	-1.28	0.11
ΔA		-0.84	0.56	1.39
L	0.0082	0.0769	0.0092	0.1678
ΔL		0.0687	0.1000	0.1586
L1	0.0075	0.0753	0.0069	0.1658
L2	0.0008	0.0016	0.0023	0.0021

Table 3. Evolution of the scores Structure (S), Amplitude (A) and Location (L) for the initial and boundary wind directions of 135º.

Table 3 shows the scores obtained by the SAL technique for the wind direction set at 135º, as function of wind intensity. The convection under sea breeze conditions is inhibited for a low threshold of synoptic wind speed, due to the fact that there is a secondary inflow of the wind along the southwest of Majorca. As in the previous case, for the weak wind intensity, the convergence of the sea breezes prevails as a trigger mechanism with a total amount of precipitation three times lower than the control simulation, attending to the score value of A = -1.

As the wind increases in intensity, the orographic forcing becomes stronger due to the fact that the incident wind is almost perpendicular to the *Serra de Tramuntana*, which is more efficient for the development of convection. For the stronger wind speed condition, the total amount of precipitation is almost the same as the control simulation. The scores (S) shows that in this case the precipitation is less peaked than the control simulation. It is interesting to note that the convective area extends outside the *Serra de Tramuntana*, it could be due to the gust front generated by the leading edge of cold air rushing down and out from the convective cells and, additionally, by the confluence of low-level atmospheric currents past the orographic obstacle.

2.4 DIRECTION 180º

Figures 13-16 of the Annex illustrate the comparative analysis between each scenario and the control simulation, and the accumulated precipitation field in twenty-four hours along with the horizontal surface wind field at 14 UTC.

WIND INTENSITY	WEAK	WEAK-MODERATE	MODERATE	STRONG
S	-0.73	-1.22	-1.84	-1.13
ΔS		-0.49	-0.62	0.71
A	-0.92	-1.39	-1.86	-0.26
ΔA		-0.47	-0.47	1.6
L	0.0552	0.0259	0.1768	0.2410
ΔL		-0.0293	0.1000	0.0642
L1	0.0546	0.0244	0.1754	0.2395
L2	0.0007	0.0015	0.0014	0.0015

Table 4. Evolution of the scores Structure (S), Amplitude (A) and Location (L) for the initial and boundary wind directions of 180º.

Table 4 shows the scores obtained by the SAL technique for the wind direction set at 180º, as function of wind intensity. The southerly synoptic flow enters easily along the meridional part of the island. This is due to the fact that significant topographic obstacles are widely spaced, and thus the orography has been noticeably smoothed with the resolution of 1 km. There is only clear evidence of convection under sea breeze conditions for the case with a weak initial and boundary wind speed. The convective areas increase along the *Serra de Tramuntana* as the wind intensity increases due to the orographic forcing, which is implied within the score (L) due to the contribution of (L_2). The total amount of precipitation increases significantly for the stronger wind speed, when the trigger mechanism is the orographic forcing, the reader is referred to observe the evolution of the score (A). On the contrary, the score (S) increases slower than (A), what means that the precipitation is less peaked than the previous scenario with a moderate wind conditions.

2.5 DIRECTION 225º

Figures 17-20 of the Annex illustrate the comparative analysis between each scenario and the control simulation, and the accumulated precipitation field in twenty-four hours along with the horizontal surface wind field at 14 UTC.

WIND INTENSITY	WEAK	WEAK-MODERATE	MODERATE	STRONG
S	-0.75	-1.03	-1.35	-1.19
ΔS		-0.28	-0.32	0.16
A	-1.26	-0.30	-0.91	-1.10
ΔA		0.96	-0.61	-0.19
L	0.1216	0.1090	0.1589	0.1516
ΔL		-0.0126	0.1000	-0.0073
L1	0.1210	0.1078	0.1571	0.1497
L2	0.0006	0.0011	0.0017	0.0019

Table 5. Evolution of the scores Structure (S), Amplitude (A) and Location (L) for the initial and boundary wind directions of 225º.

Table 5 shows the scores obtained by the SAL technique for the wind direction set at 225º, as function of wind intensity. The southwesterly synoptic wind find an open inflow through the Bay of *Palma*, reinforcing the see breeze generated by the land-sea contrast in this area of the island. On the other side of Majorca, the sea breeze formed along the Bay of *Alcudia* is only strong enough to keep the area of convergence within the island for the weak synoptic wind conditions. For the weak-moderate wind intensity, a convective cell is also

observed in the *Serra de Llevant* under orographic forcing. In addition, convection is obtained by the persistence of the sea breeze convergence. This combination of both trigger mechanisms forces that the total of precipitation is increased significantly compared with the scenario with weak wind intensity. This is quantified in the increase in the score (A) for this scenario, see Table 5.

For the scenarios with strong wind intensity as initial and boundary conditions, there is not convection under sea breeze convergence and the orographic is not relevant at all, because the incident wind has not perpendicular component to the *Serra de Tramuntana*. The precipitation is almost confined in the *Serra de Llevant* and *Cap de Formentor*. There is a strong a notably in the score (A), been the total amount of precipitation around three times lower than the control simulation.

2.6 DIRECTION 270º

Figures 21-24 of the Annex illustrate the comparative analysis between each scenario and the control simulation, and the accumulated precipitation field in twenty-four hours along with the horizontal surface wind field at 14 UTC.

WIND INTENSITY	WEAK	WEAK-MODERATE	MODERATE	STRONG
S	-0.88	-0.03	-0.87	-1.61
ΔS		0.85	-0.84	-0.74
A	-0.58	-0.26	-1.12	-1.64
ΔA		0.32	-0.86	-0.52
L	0.0873	0.0112	0.0189	0.3137
ΔL		-0.0761	0.1000	0.2948

WIND INTENSITY	WEAK	WEAK-MODERATE	MODERATE	STRONG
L1	0.0870	0.0101	0.0172	0.3129
L2	0.0003	0.0011	0.0017	0.0008

Table 6. Evolution of the scores Structure (S), Amplitude (A) and Location (L) for the initial and boundary wind directions of 270º.

Table 6 shows the scores obtained by the SAL technique for the wind direction set at 270º, as function of wind intensity. The convection under sea breeze persist for the until weak-moderate wind condition, because the westerly wind at the low troposphere is braked by the *Serra de Tramuntana*, and the inflow along the Bay of *Alcudia* together with the secondary inflow of the sea breeze located at the southeast of Majorca are strong enough to keep the convective area inland. The total amount of precipitation gradually decreases as the initial conditions increase, due to the fact that the orographic forcing is not relevant to the convection. The incident wind has an angle of approximately 45º with respect to the *Serra de Tramuntana*, therefore the perpendicular component is not strong enough to lead convection under orographic forcing. Hence, there are less precipitation for the moderate and strong wind conditions, see the negative evolution of the score (A), table 6. There is a displacement to the east and a decrease in the convective area as the wind conditions increase, see the evolution of the score (L).

2.7 DIRECTION 315º

Figures 24-28 of the Annex illustrate the comparative analysis between each scenario and the control simulation, and the accumulated precipitation field in twenty-four hours along with the horizontal surface wind field at 14 UTC.

WIND INTENSITY	WEAK	WEAK-MODERATE	MODERATE	STRONG
S	-0.63	-0.48	-0.82	-1.20
ΔS		0.15	-0.34	-0.38
A	-0.65	-0.65	-1.17	-0.35
ΔA		0	-0.52	0.82
L	0.0037	0.0196	0.0199	0.2685
ΔL		0.0159	0.1000	0.2486
L1	0.0335	0.0189	0.0186	0.2676
L2	0.0002	0.0007	0.0013	0.0009

Table 7. Evolution of the scores Structure (S), Amplitude (A) and Location (L) for the initial and boundary wind directions of 315º.

Table 7 shows the scores obtained by the SAL technique for the wind directions set at 315º, as function of wind intensity. For the scenario with the lowest initial wind speed conditions, the northwesterly wind at 14 UTC impinges perpendicularly to the *Serra de Tramuntana* and is not able to overpass the mountain range, see Fig. 25b. As the wind speed increases, downdraft acceleration is observed leewards. These balances among the instability in the area, the perpendicular component of the incident wind and the height of the mountain range are expressed through the Froude Number. There is a direct relation between the instability and the wind speed, given that in our experiments the height of the mountain is fixed. If the instability increases, the convection under orographic forcing is possible for lower initial wind intensities. On the contrary, the higher are the stability conditions, the higher is the wind speed threshold necessary for the wind to cross the mountain, and more downdraft leeward acceleration is also expected.

Although the *Serra de Tramuntana* implies much resistance to the northwesterly winds, the convergence under sea breeze conditions is not observed for all scenarios. This is because the downdraft acceleration experience leewards is stronger than the see breeze generated in the south of the island. For the highest initial and boundary wind conditions the convection under orographic forcing leads to convective precipitation in the main reliefs of Majorca. To summarize, the precipitation decreases until moderate wind condition, where there is an inflection point due to orographic forcing, see the evolution of the score (A), table 7.

2.8 DIRECTION 360º

Figures 29-32 of the Annex illustrate the comparative analysis between each scenario and the control simulation, and the accumulated precipitation field in twenty-four hours along with the horizontal surface wind field at 14 UTC.

WIND INTENSITY	WEAK	WEAK-MODERATE	MODERATE	STRONG
S	-1.28	-0.60	-1.90	-1.56
ΔS		0.68	-1.3	0.34
A	-1.03	-0.97	-1.97	-1.15
ΔA		0.06	-1	0.82
L	0.1559	0.0042	0.0261	0.0190
ΔL		-0.1517	0.1000	-0.0071
L1	0.1553	0.0031	0.0244	0.0175
L2	0.0005	0.0011	0.0016	0.0015

Table 8. Evolution of the scores Structure (S), Amplitude (A) and Location (L) for the initial and boundary wind directions of 360º.

Table 8 shows the scores obtained by the SAL technique for the wind direction set at 360º, as function of wind intensity. The north wind is a common scenario which is known as *Tramuntana.* It occurs when there are low pressures in the north of Italy and high pressures towards the southwest of France or the Iberian Peninsula. Generally, the wind strikes east of Majorca.

The convergence under sea breeze conditions is observed for the weak and weak-moderate wind conditions. Attending to the evolution of the score (A), see Table 8, the total amount of precipitation is almost three times lower than the control simulation. Subsequently, there is a significant decrease of precipitation for the moderate wind condition. Finally, the convection under orographic forcing starts under the strong wind conditions, over the *Serra de Tramuntana*, leading to an increase in the precipitation.

2.9 SAL DIAGRAM

In Figure 65 of the Annex, a SAL diagram has been plotted in order to summarize the thirty-two simulations with orography. If the score (A) is attended, the amount of precipitation of the simulations is less than the control simulation, except for the case with the south-easterly wind with an intensity of 14.1 m/s, where the orographic forcing was relevant. There is a relation between (A) and (S) since most of the points are clustered close to the bisecting line of the (A) and (S) negative axes. This is due to the fact that all the precipitation events are convective. If the trigger mechanism was only the convergence of the sea breezes, it would be expected that the convective cells decrease in size and move away from the center of the island, or even that they vanish. Therefore, a larger value of (L) is expected when the value of (A) decreases, but it is not observed in Figure 65 due to the influence of the orography as a trigger mechanism.

This project has been extended in order to confirm all the conclusions that have been reached so far. The thirty-two simulations have been run again with the orography set to zero.

3 SIMULATIONS WITHOUT OROGRAPHY

The thirty-two simulations have been classified according to the trigger mechanism of the convection into two groups: the first group includes sixteen simulations with initial wind intensities of 3.5 m/s and 7.1 m/s, where the convergence under sea breeze conditions dominates over the orographic forcing as a trigger mechanism. The opposite happens in the second group which includes the remaining sixteen simulations with initial wind intensities of 10.6 m/s and 14.1 m/s.

The Amplitude score (A) has been analyzed in order to study the trend of total amount of precipitation in both groups (Table 9, where the two groups of simulations are emphasized in colors; also note two cases that are an exception to the above general rule).

AMPLITUDE	1st group		2nd group	
ff/dd	WEAK	WEAK-MODERATE	MODERATE	STRONG
45º	0.72	0.13	0.30	-0.80
90º	0.78	0.87	-0.94	-2.00
135º	0.84	1.76	-1.69	-2.00
180º	0.79	1.19	-1.23	-2.00
225º	1.36	0.20	-0.32	-1.32
270º	0.63	0.29	-1.92	-2.00
315º	0.14	-0.07	-1.78	-2.00
360º	0.83	0.24	-0.79	-2.00

Table 9. Evolution of the Amplitude score (A) for each simulation with the orography set to zero, taking its counterpart with orography as a reference. Positive values of (A) in red and negative values of (A) in green.

The total amount of precipitation increases in the scenarios of the 1st group (positives values of (A) in Table 9) except for the case with initial wind conditions that have a direction of 315º and intensity of 7.1 m/s. The sea breezes can penetrate inland along the island shores, intensifying the convergence area and bringing more moisture, causing a larger and more intense convective precipitation area. In Fig. 66 of the Annex, a SAL diagram has been plotted in order to summarize the sixteen simulations of the 1st group, the most of them are grouped into the quadrant with positives values of (A) and (S), confirming the general increase in precipitation.

On the contrary, the total amount of precipitation decreases in the scenarios of the 2nd group (see negatives values of (A) in Table 9) except for the one with an initial wind conditions with a direction of 45º and intensity of 10.6 m/s. This is due in fact that with the orographic height set to zero above sea level, the orographic forcing is eliminated. There are some scenarios where a residual convective precipitation is found downstream of the island and it always appears when the synoptic wind is strong enough to clearly cross the island. It is reflected in the surface wind at 14 UTC as a deceleration of the synoptic wind field over the island and some curved flow and convergence downstream, being a consequence of the differential land-sea diurnal heating (and friction). In Fig. 67 of the Annex, a SAL diagram has been plotted in order to summarize the sixteen simulations of the 2nd group, where the most of them are grouped into the quadrant with negative values of (A) and (S), confirming the general decrease in precipitation.

The reader is referred to Figures 33-64 in the Annex, in order to make a comparative analysis between each scenario and its counterpart with orography and in order to analyze the accumulated precipitation field in twenty-four hours and its relation with the horizontal surface wind field at 14 UTC.

The evolution of the score (S) has been summarized in Table 10. It is expected to find positive values in the 1st group, due to the increase of precipitation when the convection occurs under sea breeze convergence. On the contrary, negative values of (S) are expected in the 2nd group, explained by the decrease of precipitation. (The two groups of simulations are emphasized in colors; note also a few cases that are an exception to the above general rule).

STRUCTURE	1st group		2nd group	
ff/dd	WEAK	WEAK-MODERATE	MODERATE	STRONG
45º	0.37	-0.36	0.20	0.28
90º	0.35	1.41	0.64	NaN
135º	1.22	1.84	-1.32	NaN
180º	0.60	1.15	-0.94	NaN
225º	0.63	0.46	0.30	-0.20
270º	1.27	0.18	-1.71	NaN
315º	0.32	0.01	-1.37	NaN
360º	1.59	0.25	-0.57	NaN

Table 10. Evolution of the Structure score (S) for each simulation with the orography set to zero, taking as a reference its counterpart with orography. Note: NaN are the result of null precipitation fields.

If the amount of precipitation was keep constant for each scenario, then the score (A) would be equal to 0. Then, it would be enough to study the sign of (S) in order to determine if the precipitation without orography is more peaked (S < 0) or widespread (S>0). But the situation is more complex to analyze in our case because there are strong variations in A. Therefore, the difference between [A-S] is summarized in Table 11 with the aim of highlighting the scenarios with large differences. For these scenarios, we can conclude for the precipitation field of the simulation without orography that, it is more peaked for positive values of [A -S] (S<0), and it is more widespread for negative values of [A-S] (S>0).

[A-S]	1st group		2nd group	
ff/dd	WEAK	WEAK-MODERATE	MODERATE	STRONG
45º	0.35	0.49	0.5	-1.08
90º	0.43	-0.54	-1.58	NaN
135º	-0.38	-0.08	-0.37	NaN
180º	0.19	0.04	-0.29	NaN
225º	0.73	-0.26	-0.62	-1.12
270º	-0.64	0.11	-0.21	NaN
315º	-0.18	-0.08	-0.41	NaN
360º	-0.76	-0.01	-0.22	NaN

Table 11. Evolution of the differences between the score (A) and (S) for each simulation with the orography set to zero, taking as a reference its counterpart with orography. Note: NaN are the results of null precipitation fields.

(In Table 11, The difference in [A-S] above a threshold of |0.4| are emphasized in colors; positive values in red and negative values in green). Analyzing all scenarios without orography together, there is a tendency for more peaked precipitation with respect to their counterparts with orography (ie. dominance of negative values in Table 11). On the one hand, there are a few of them which the precipitation is clearly more widespread, attending to the scenarios marked in red in Table 11. On the other hand, the scenarios with more peaked precipitation are more frequently and intensive, and are marked in green in Table 11.

CONCLUSION

Thirty-two different ideal and homogeneous initial and boundary conditions were simulated, with the aim of isolating as much as possible the interactions between the synoptic wind field and the convergence generated by the diurnal sea breeze. All the simulations have been run under certain instability conditions provided by the atmospheric sounding, and assuming that the interactions which take place in the atmosphere have a nonlinear character.

It has been detected that there is a threshold from which orographic forcing dominates the development of convection, to the detriment of the convergence of sea breeze. The complex orography of Majorca determines the wind inflow, limiting the intensity and the moisture supply of the convergence at low levels. For the eight possible scenarios simulated, with low initial and boundary wind speed conditions of 3.5 m/s, the convergence of sea breeze undergoes a slight shift but still remains within the island. It is for the scenarios with 7.1 m/s, when the convergence is only keeping inland, for the directions where the wind at low levels experiences a slowdown when it interacts with the relief, it happens at the north, northeast, west and southwest winds. On the contrary, for the initial and boundary wind speed conditions of 10. 6 m/s and 14.1 m/s, most of the convective precipitation obtained as a result of the orographic forcing, which efficiency depends on the angle between the incident wind and the main mountain ranges of the island, being a reason why the southeast and northwest winds, with an initial and boundary wind speed of 14.1 m/s shows higher values of precipitation, which is quantified by the amplitude score. The wind incident is almost perpendicular to the *Serra de Tramuntana* mountain range. It is also relevant for the northwest wind the second main relief of Majorca, the *Serra de Levante*. The south wind shows high values of precipitation, although the incident wind is not perpendicular to the main mountain range, but the convection is still very effective in the area of *Serra de Tramuntana* located further south. This is due to the incident winds impinging directly from the sea.

The results of the thirty-two simulations obtained with the orography set in one meter above sea level, for the same initial and boundary conditions supports that; it is obtained under certain instability conditions, when the trigger mechanism predominant is the convergence of the sea breeze, the accumulative convective precipitation increases notably. This is due to the fact that the sea breeze can form on all the shores of the island, which increases the moisture supply and the intensity of the convergence at low levels. On the contrary, less accumulated convective precipitation is obtained when the trigger mechanism predominant is the orographic forcing, not having precipitation when there is not any slowdown of the wind, and the only trigger mechanism is the orographic forcing.

Majorca is an ideal laboratory for studying mesoscale phenomena, due its characteristics, size and location. It has set a certain condition of instability in this project, but by using the same domain, a line of study could be opened with the aim of analyzing other mesoscale processes, as a result of the variations of the vertical stratification. If an inversion is created at the height of the average summits of the *Serra de Tramuntana*, the incident wind with certain intensity could lead to mountain waves, or leeward downdrafts. The relation among the perpendicular horizontal component to the mountain range (U), the height of the mountain range (H) and the Brünt Väisälä frecuency (N), is given by the Froud Number (i).

$$F_r = \frac{U}{HN} \quad (i)$$

Another interesting line of work could be to study the influence of the mountain and valley breeze generated by differential heating on the slopes of the major mountain ranges of the island, mainly the *Serra de Tramuntana*. Perhaps a higher resolution domain would be needed in order to detect the component of the wind at low levels, which could be affected during the diurnal heating.

BIBLIOGRAPHY

Alomar G., M. Grimal and M. Laita, 2004. La percepción geográfica del régimen de brisas en Mallorca de la experiencia directa a los datos instrumentales. In: *El Clima, entre el Mar y la Montaña* (García Codrón, J. C. Diego Liaño, C., Arróyabe Hernáez, P. F., Garmendia Pedraja, C. and Rasilla Álvarez, D., Eds.). AEC Publications (Asociación Española de Climatología), Santander, 551–559.

Alonso S., A. Jansà, C. Ramis, 1983. Una simulación numérica de la brisa en la Isla de Mallorca. En: *VI Asamble Nacional de Geodesia y Geofísica.*

Brown, B.G., R.R. Bullock, C.A. David, J.H. Gotway, M.B. Chapman, A. Takacs, E. Gilleland, K. Manning, J. Mahoney, 2004. New verification approaches for convective weather forecasts. *11th Conf. Aviation, Range, and Aerospace Meteorology, 4-8 Oct 2004, Hyannis, MA.*

Azorin C.. J.A. Guijarro, R.Baena Calatrava, A. Jansà, 2007. Sea breeze convergence and convective cloud frequencies from AVHRR data over the isle of Mallorca. *8 European conference on Applications of Meteorology. San Lorenzo del Escorial.*

Davis, C., B. Brown, and R. Bullock, 2006a. Object-based verification of precipitation forecasts. Part I: Methods and application to mesoscale rain areas. *Mon. Wea. Rev., **134**, 1772-1784.*

Ebert, E.E. and J.L. McBride, 2000. Verification of precipitation in weather systems: Determination of systematic errors. *J. Hydrology, **239**, 179-202.*

González J, Guijarro JA, Jansá A (1998). Caracterización de la brisa en Mallorca. IX Asamblea Nacional de Geodesia y Geofísica (Almería, 9-13/Feb):347-?

Jolliffe, I.T., and D. B Stephenson, 2003. Forecast Verfication: A practitioner's Guide in Atmospheric Science. Wiley and Sons, 240 pp

Lack, S., G.L. Limpert, and N.I. Fox, 2010. An object-oriented multiscale verification scheme. *Wea. Forecasting*, **25**, 79-92.

Michaes, A.C., N.I. Fox, S.A. Lack and C.K. Wikle, 2007. Cell identification and verification of QPF ensembles using shape analysis techniques. *J. Hydrol.*, **343**, 105-116.

Marzban, C. and S. Sandgathe, 2008. Cluster analysis for object-oriented verification of fields: A variation. *Mon. Wea. Rev.*, **136**, 1013-1025.

Nachamkin, J.E., 2004. Mesoscale verification using meteorological composites. *Mon. Wea. Rev.*, **132**, 941-955.

Nurmi P., 2003. Recommendations on the verification of the local weather forecast (at ECMWF Member States).

Ramis C., and S. Alonso, 1988. Sea breeze convergence line in Majorca: A satellite observation", Weather, 43, pp. 288-293.

Ramis C., A. Jansà, and S. Alonso, 1990. See breeze in Mallorca: A numerical study. *Meteorology and Atmospheric Physics*, 42, pp. 249-258.

Ramis c., R. Romero, 1995. A first numerical simulation of the development and structure of the sea breeze on the island of Mallorca. *Ann. Geophy.*, 13, pp. 981-994.

Ramis C., 1998. "L'embat a l'illa de Mallorca". *TERRITORIS, Revista del Departament de Ciències de la Terra, Universitat de les Illes Balears*, pp. 243-274.

Romero, R., 1998. Numerical simulation of mesoscale processes in the western Mediterranean: Environmental impact and natural hazards. Universitat de les Illes Balears (Spain), July. *Ph. D. Dissertation.*

Romero, R., and C. Ramis, 1996: A numerical study on the transport and diffusion of coastal pollutants during the breeze clycle in the island of Mallorca. *Ann. Geophy.*, **14**, 351-363

Wernli H., and M. Sprenger, 2007. Identification and ERA-15 climatology of potential vorticity streamers and cutoffs near extratropical tropopause. American Meteorological Society. *64,* 1569-1586.

Wernli H., M. Paulat, M. Hagen and C. Frei, 2008. SAL- A Novel Quality Measure for the Verification of Quantitative Precipitation Forecasts. American Meteorological Society. *136,* 4470–4487.

ANNEX

SIMULATIONS WITH OROGRAPHY
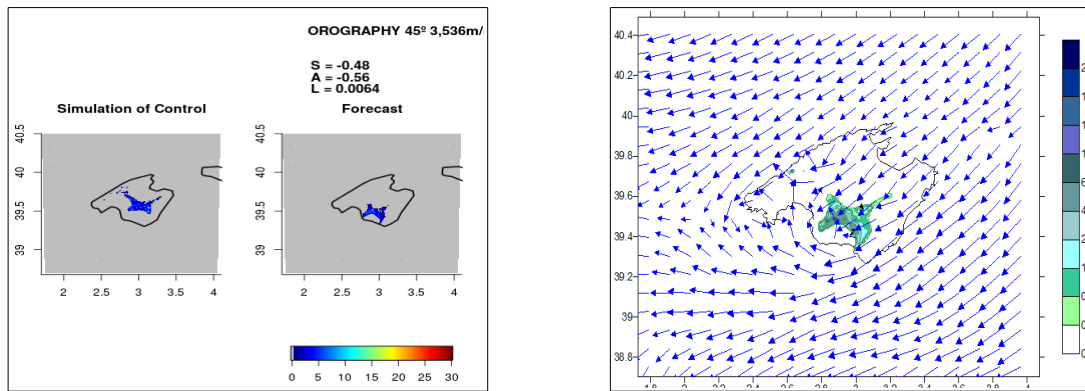
Figure 1
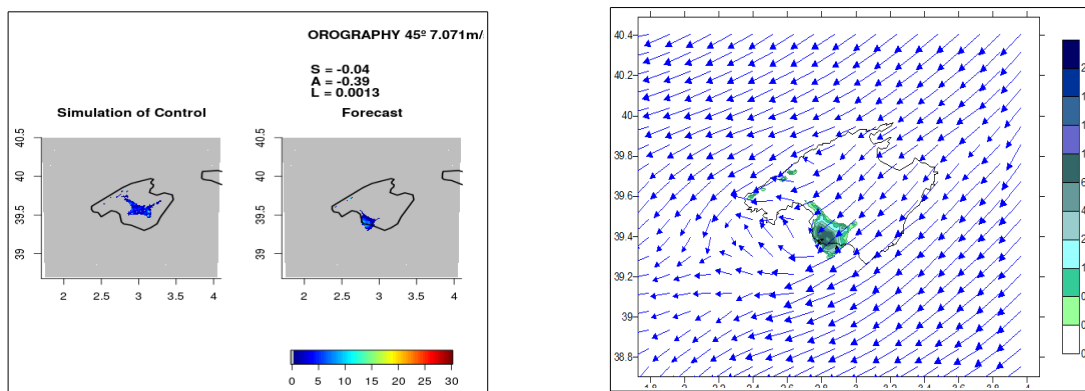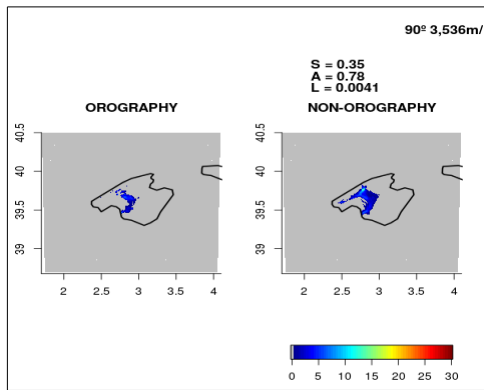

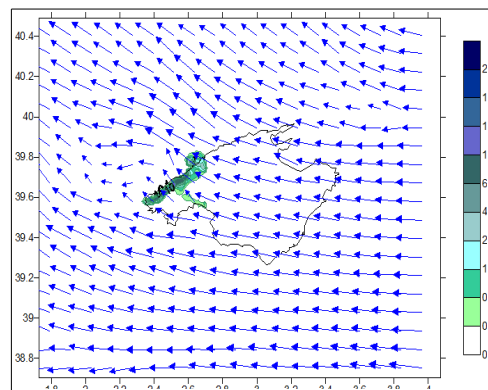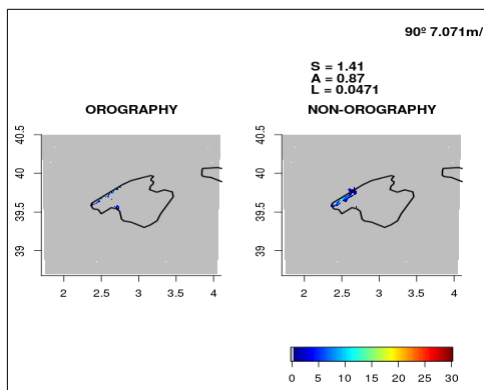Figure2
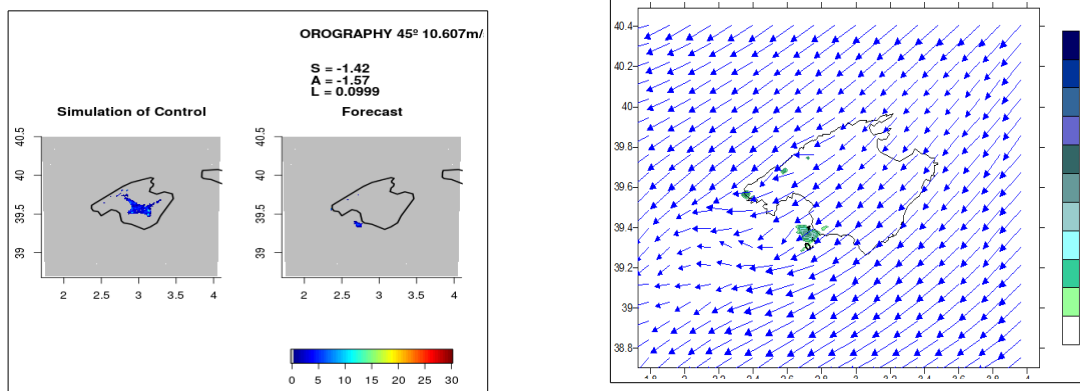
Figure 3
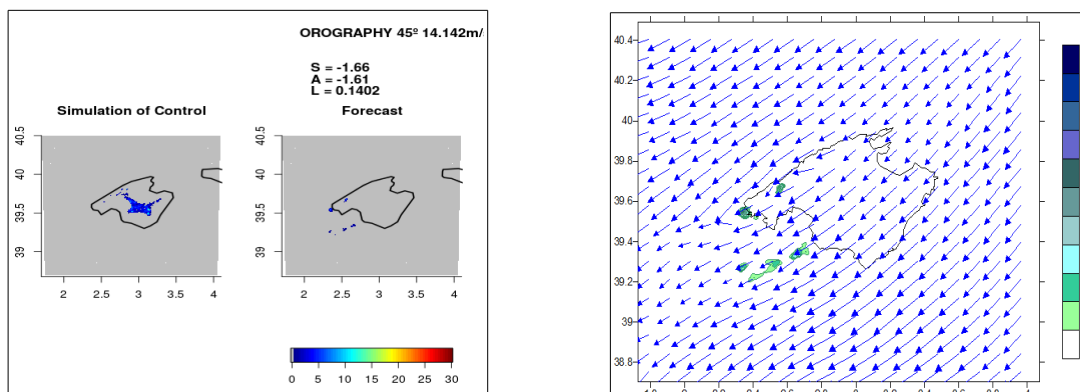
Figure 4

The initial and boundary wind direction conditions have been established at 45º, with different wind intensities: 1) ff = 3.5 m/s, 2) ff = 7.1 m/s, 3) ff = 10.6 m/s, 4) ff = 14.1 m/s. In Fig. 1-4, the comparison of the accumulated precipitation field in twenty-four hours between each simulation and the control simulation is plotted on the left and the accumulated precipitation field with the wind field at 14 UTC is plotted on the right. For the wind field, a vector length of 1 cm (⟶) corresponds to 5 m/s, 7.5 m/s, 10 m/s and 12.5 m/s for each Fig. 1-4 respectively.
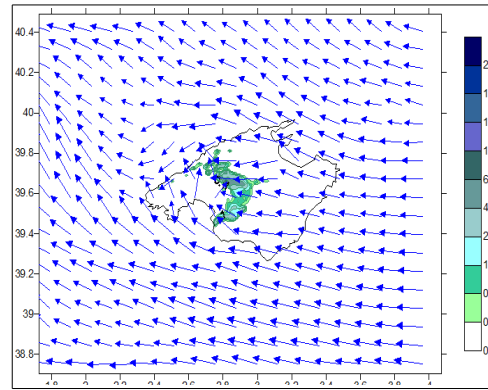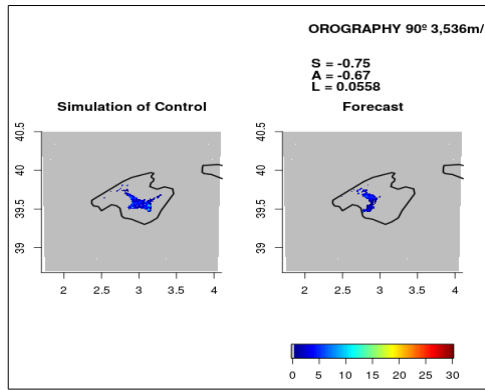
Figure 5
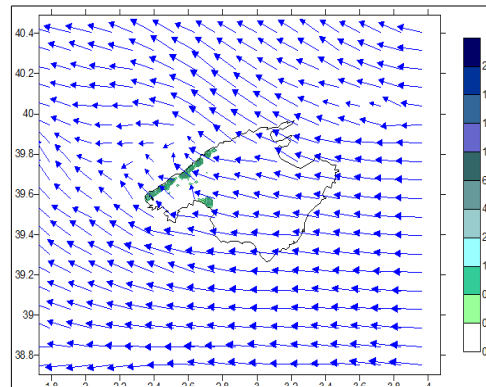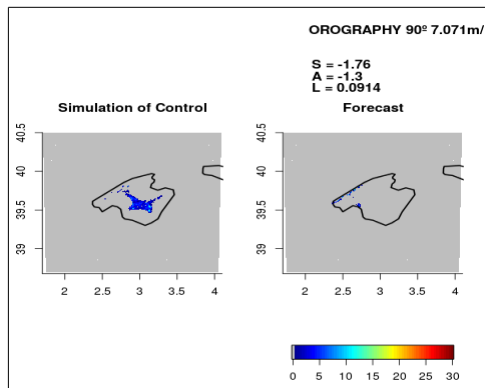
Figure 6
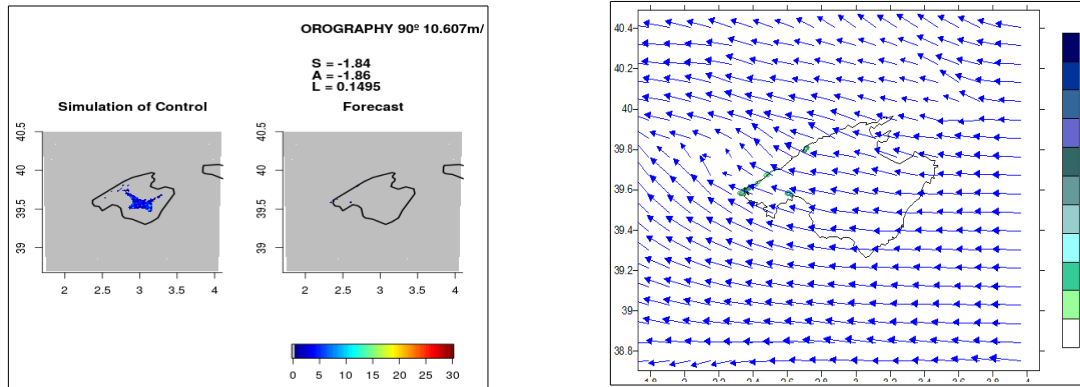
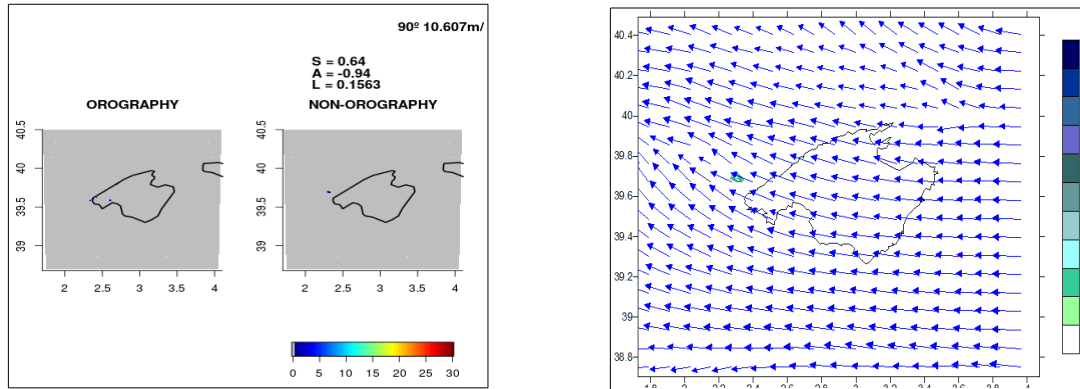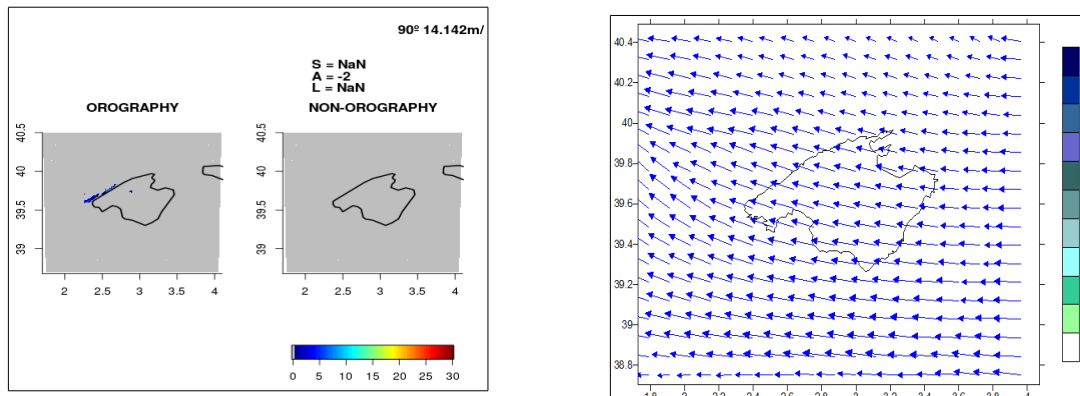Figure 7
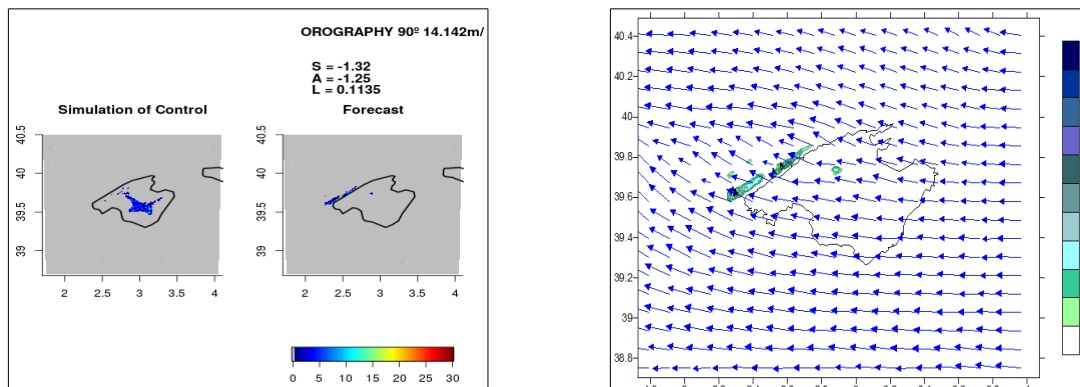
Figure 8

The initial and boundary wind direction conditions have been established at 90º, with different wind intensities: 1) ff = 3.5 m/s, 2) ff = 7.1 m/s, 3) ff = 10.6 m/s, 4) ff = 14.1 m/s. In Fig. 5-8, the comparison of the accumulated precipitation field in twenty-four hours between each simulation and the control simulation is plotted on the left and the accumulated precipitation field with the wind field at 14 UTC is plotted on the right. For the wind field, a vector length of 1 cm (⟶) corresponds to 5 m/s, 7.5 m/s, 10 m/s and 12.5 m/s for each Fig. 5-8 respectively.
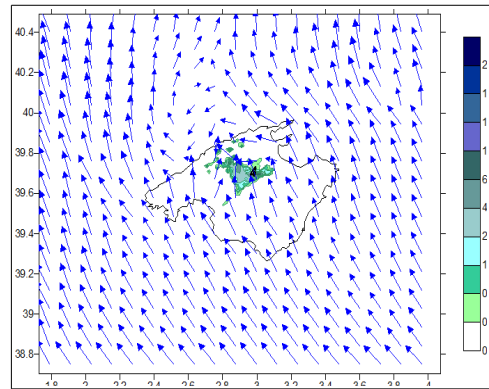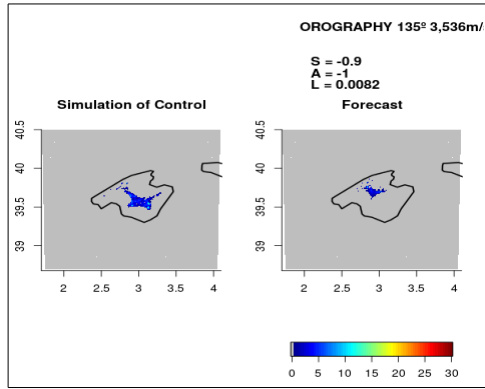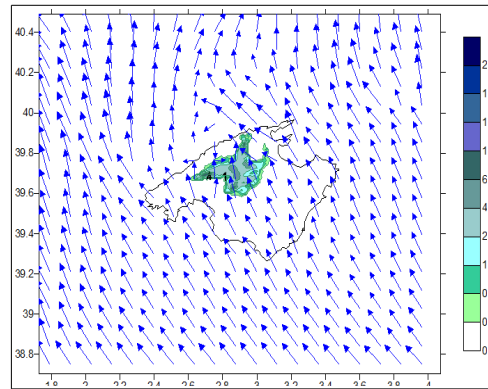
Figure 9
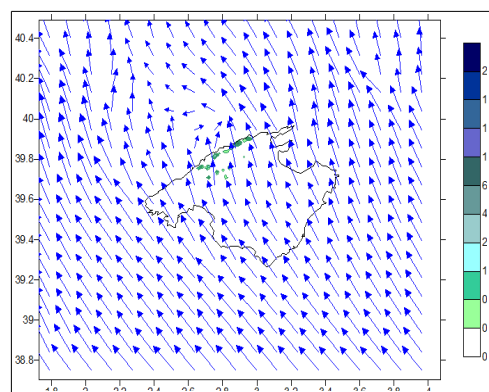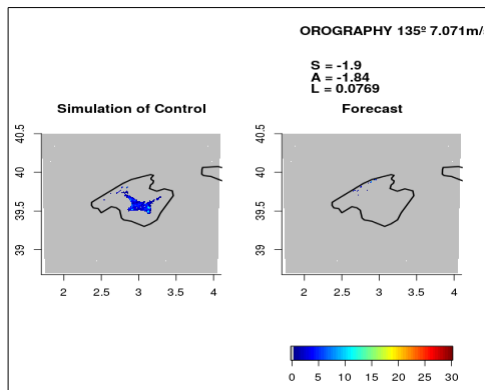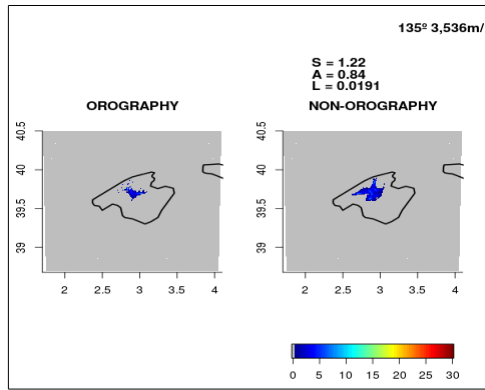

Figure 10
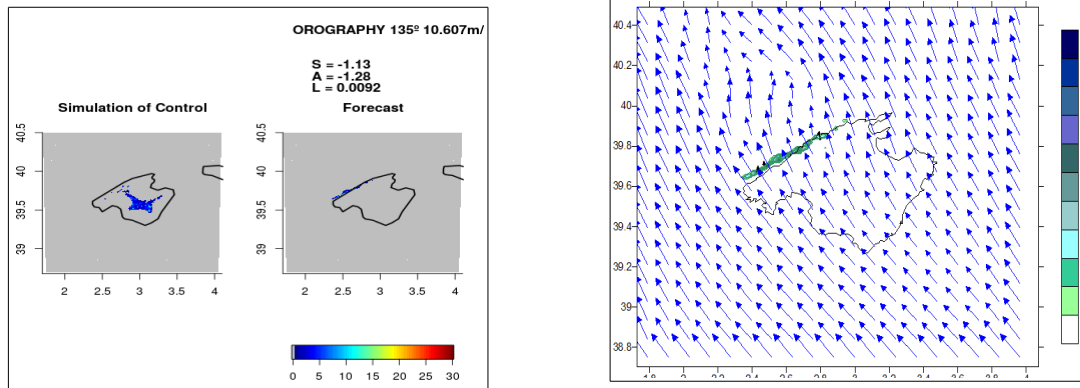
Figure 11
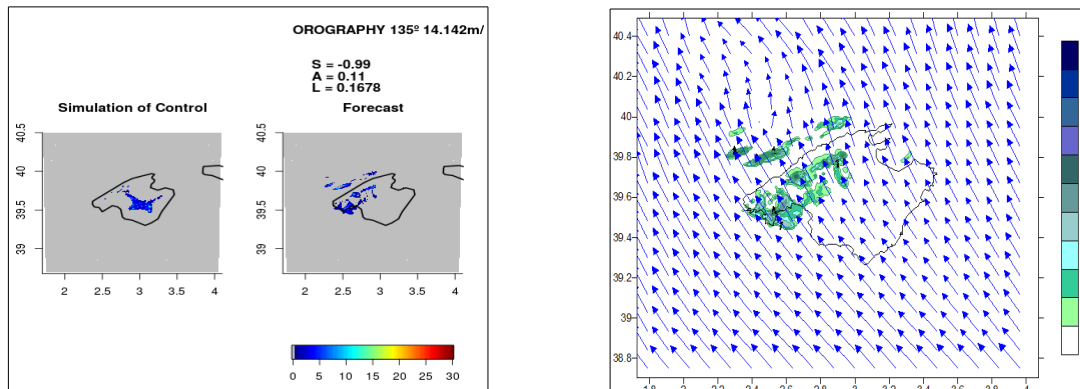
Figure 12

The initial and boundary wind direction conditions have been established at 135º, with different wind intensities: 1) ff = 3.5 m/s, 2) ff = 7.1 m/s, 3) ff = 10.6 m/s, 4) ff = 14.1 m/s. In Fig. 9-12, the comparison of the accumulated precipitation field in twenty-four hours between each simulation and the control simulation is plotted on the left and the accumulated precipitation field with the wind field at 14 UTC is plotted on the right. For the wind field, a vector length of 1 cm (➔) corresponds to 5 m/s, 7.5 m/s, 10 m/s and 12.5 m/s for each Fig. 9-12 respectively.
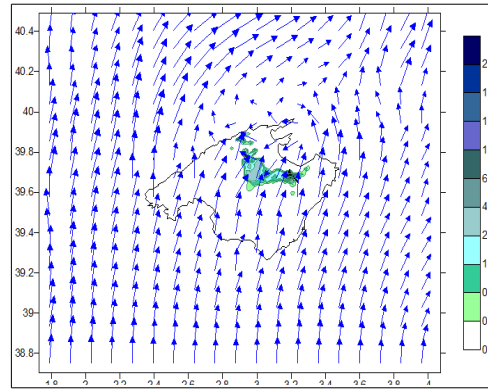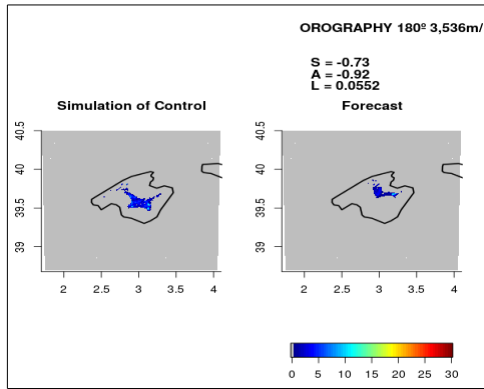
Figure 13
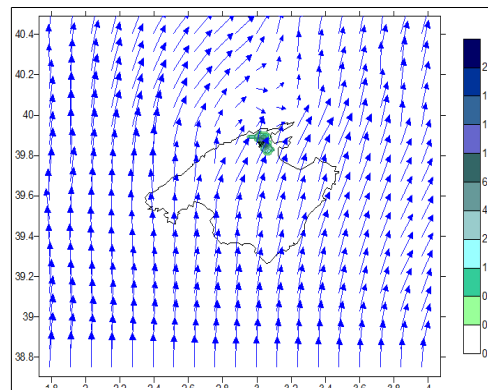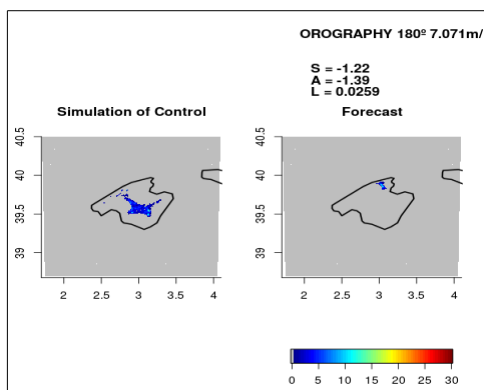
Figure 14
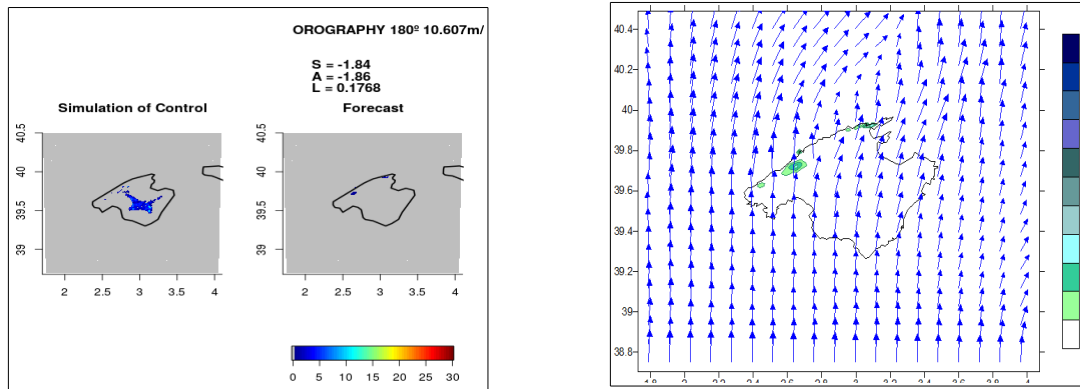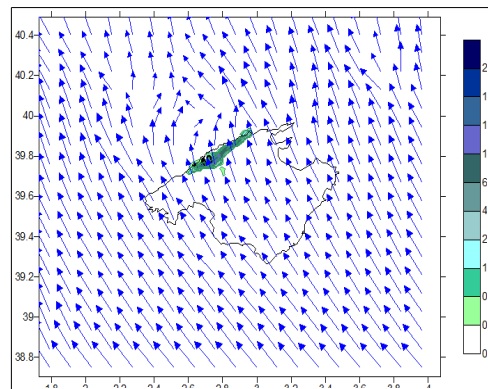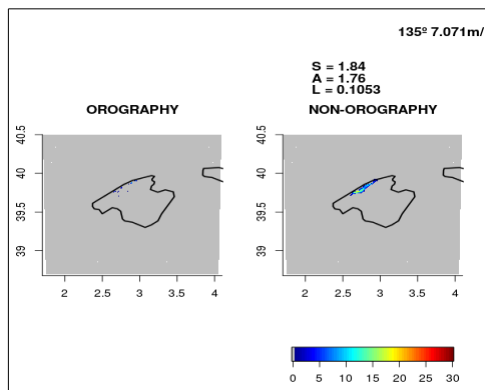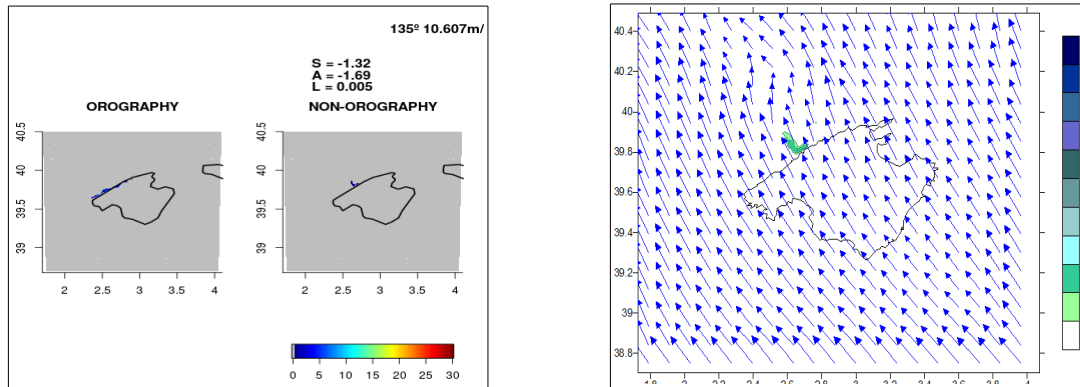
Figure 15
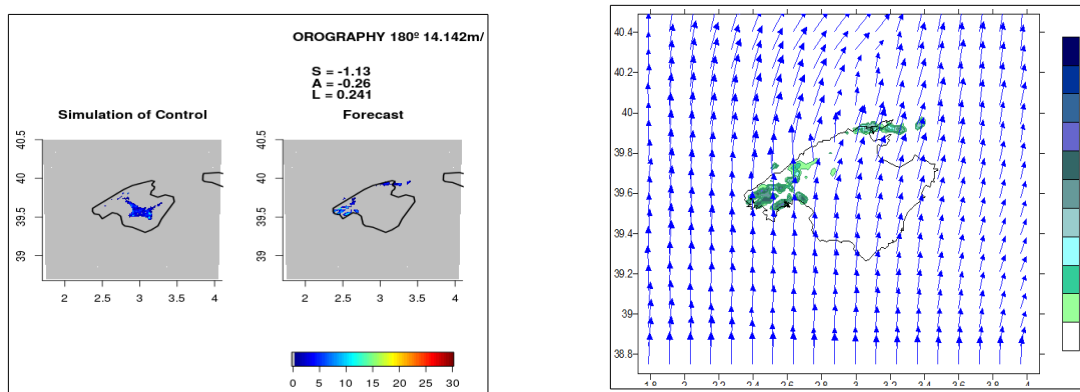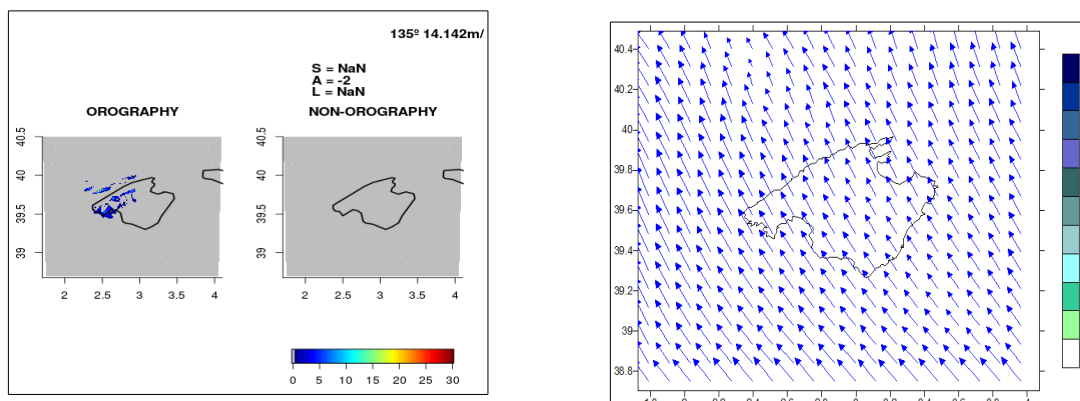

Figure 16

The initial and boundary wind direction conditions have been established at 180º, with different wind intensities: 1) ff = 3.5 m/s, 2) ff = 7.1 m/s, 3) ff = 10.6 m/s, 4) ff = 14.1 m/s. In Fig. 13-16, the comparison of the accumulated precipitation field in twenty-four hours between each simulation and the control simulation is plotted on the left and the accumulated precipitation field with the wind field at 14 UTC is plotted on the right. For the wind field, a vector length of 1 cm (⟶) corresponds to 5 m/s, 7.5 m/s, 10 m/s and 12.5 m/s for each Fig. 13-16 respectively.
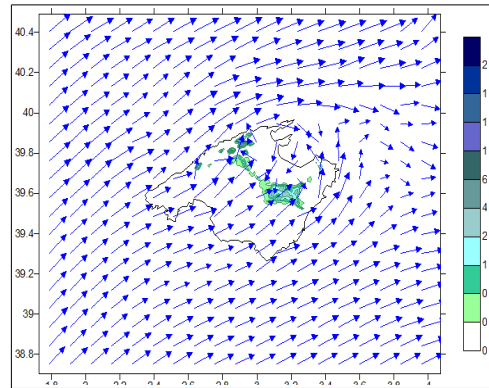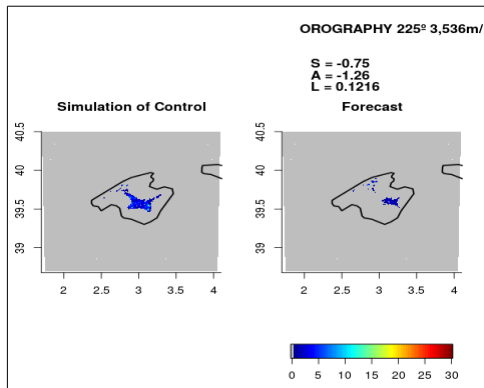
Figure 17
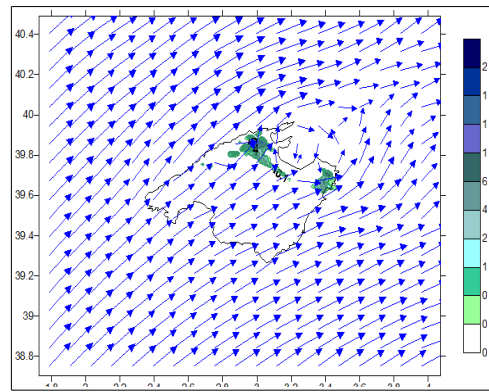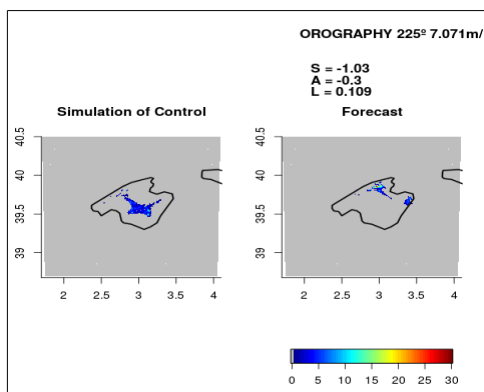
Figure 18
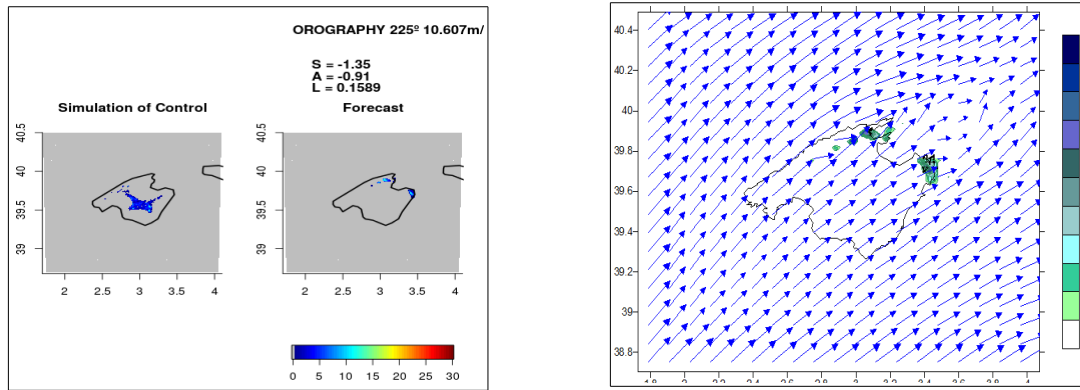
Figure 19
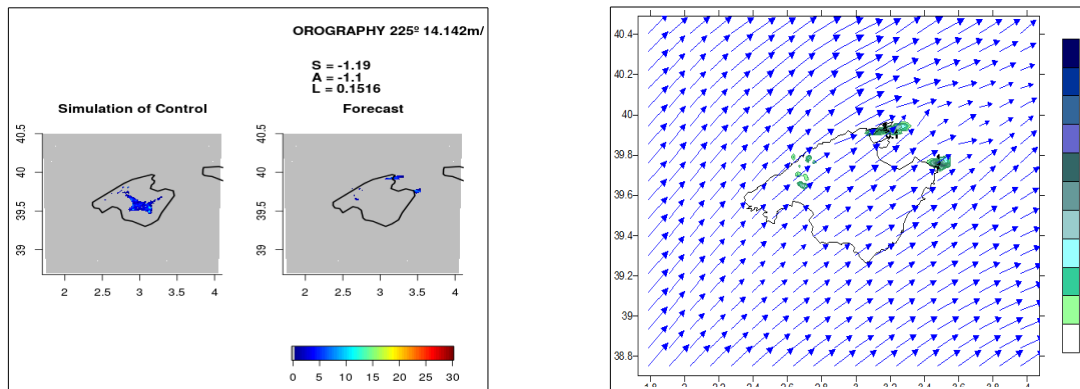
Figure 20

The initial and boundary wind direction conditions have been established at 225º, with different wind intensities: 1) ff = 3.5 m/s, 2) ff = 7.1 m/s, 3) ff = 10.6 m/s, 4) ff = 14.1 m/s. In Fig. 17-20, the comparison of the accumulated precipitation field in twenty-four hours between each simulation and the control simulation is plotted on the left and the accumulated precipitation field with the wind field at 14 UTC is plotted on the right. For the wind field, a vector length of 1 cm (⟶) corresponds to 5 m/s, 7.5 m/s, 10 m/s and 12.5 m/s for each Fig. 17-20 respectively.
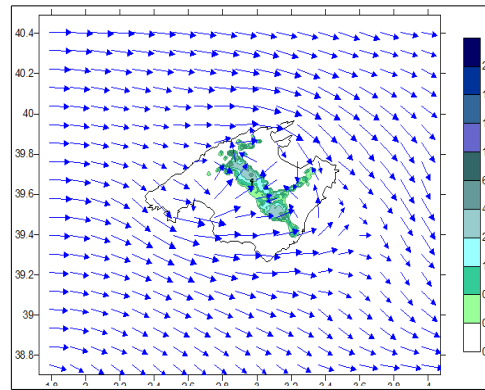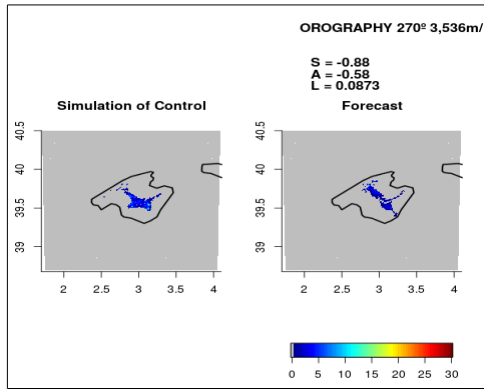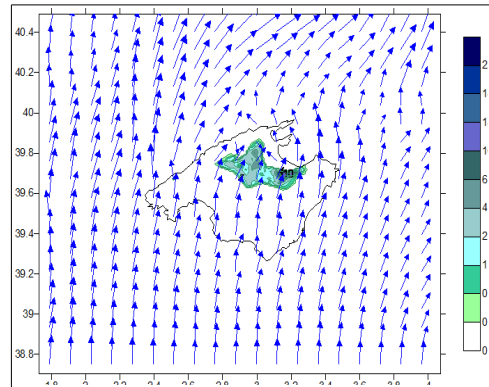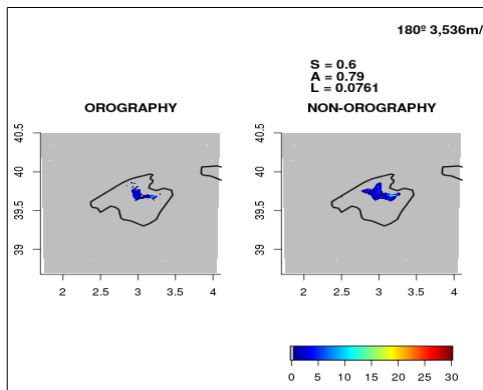
Figure 21
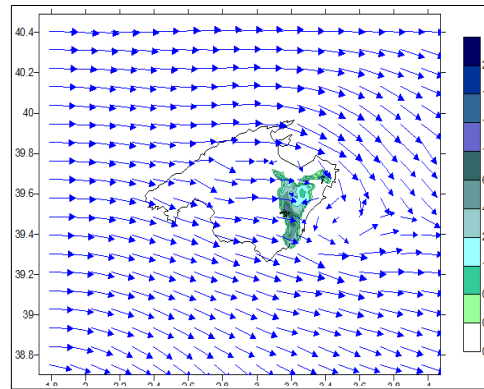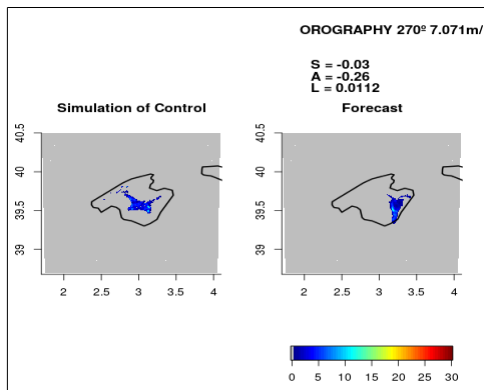
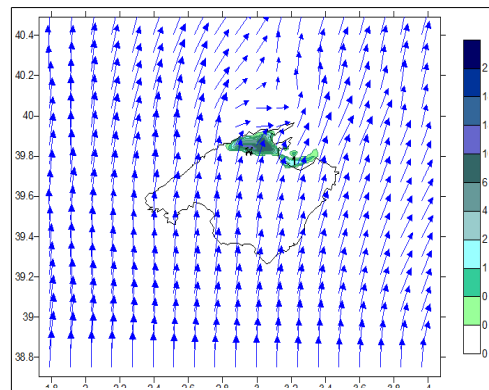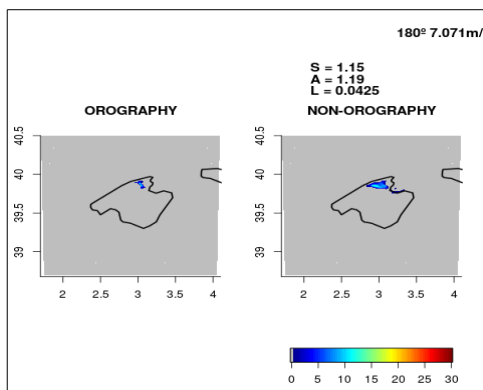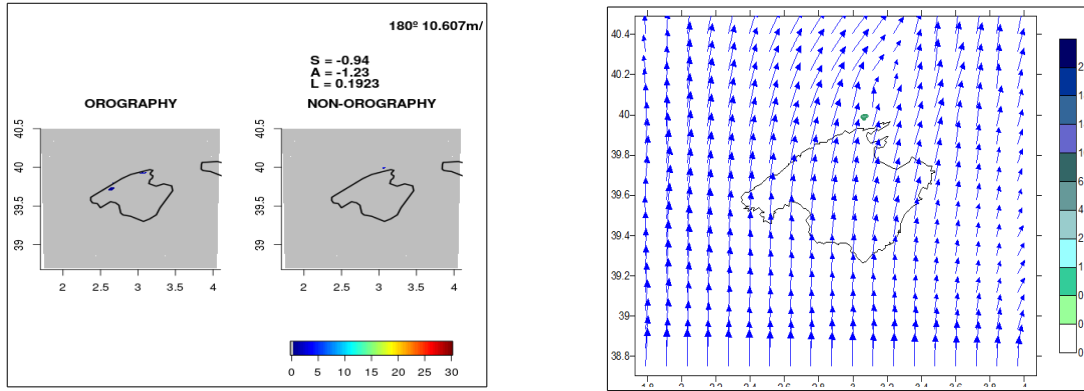Figure 22
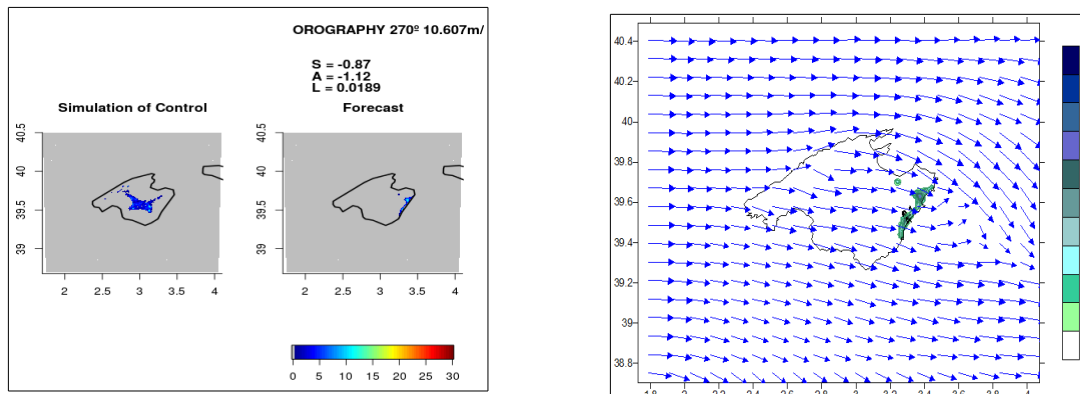
Figure 23
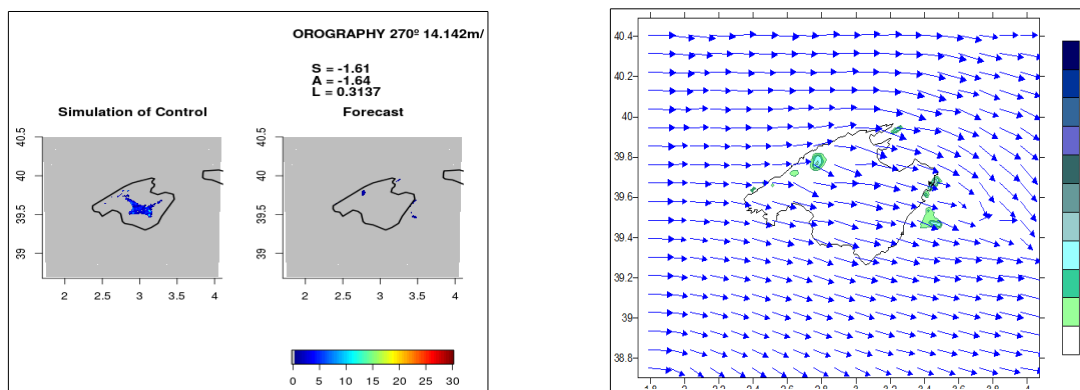
Figure 24

The initial and boundary wind direction conditions have been established at 270º, with different wind intensities: 1) ff = 3.5 m/s, 2) ff = 7.1 m/s, 3) ff = 10.6 m/s, 4) ff = 14.1 m/s. In Fig. 21-24, the comparison of the accumulated precipitation field in twenty-four hours between each simulation and the control simulation is plotted on the left and the accumulated precipitation field with the wind field at 14 UTC is plotted on the right. For the wind field, a vector length of 1 cm (⟶) corresponds to 5 m/s, 7.5 m/s, 10 m/s and 12.5 m/s for each Fig. 21-24 respectively.
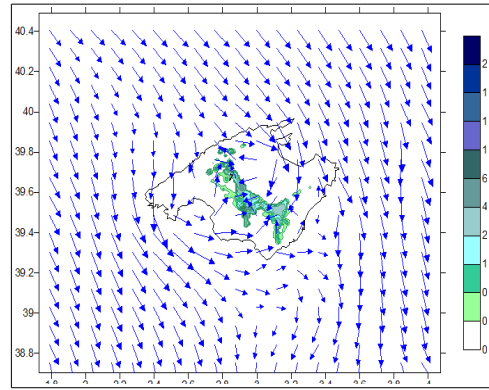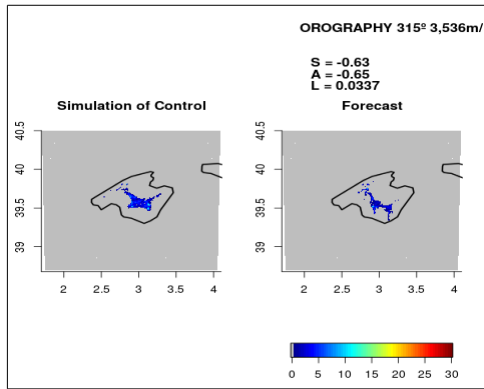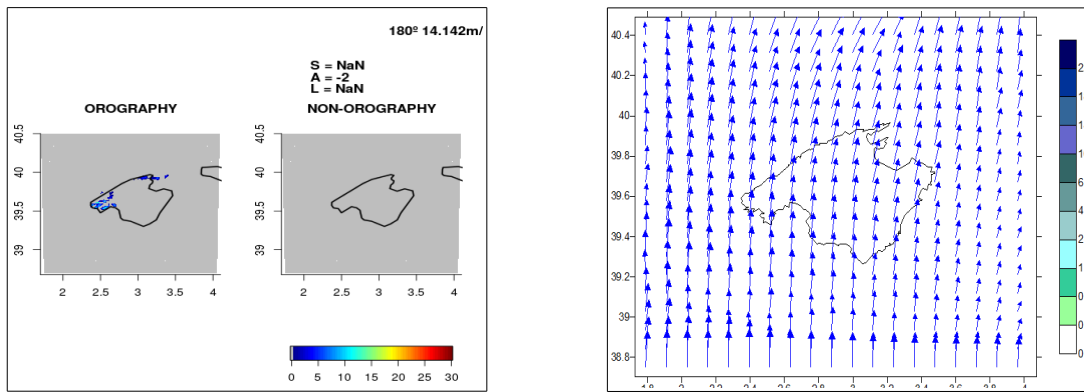
Figure 25
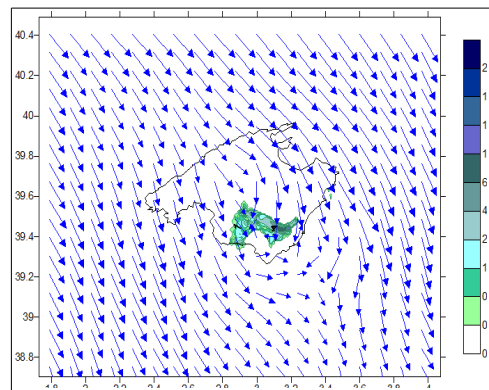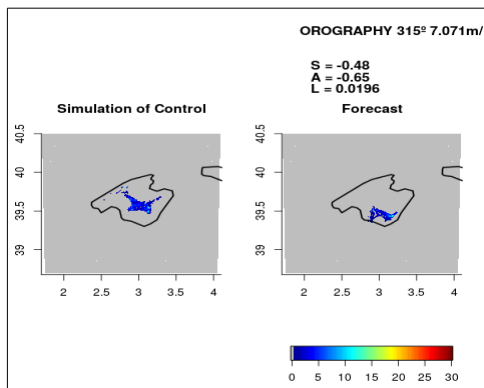
Figure 26
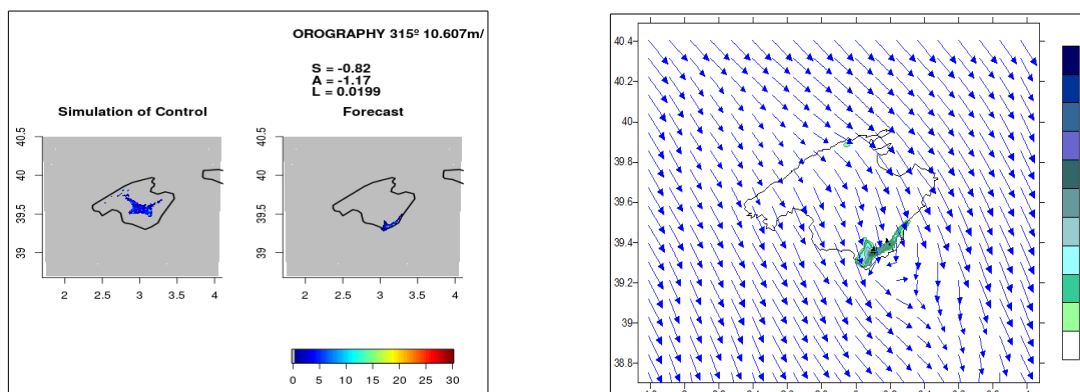
Figure 27
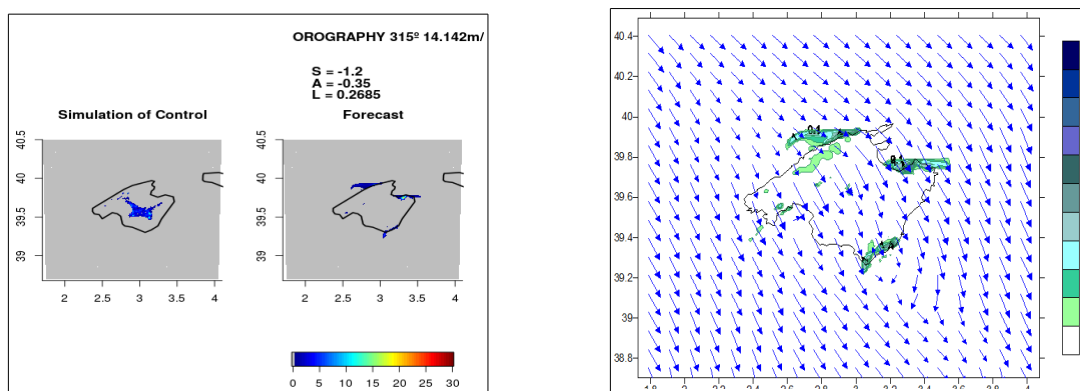
Figure 28

The initial and boundary wind direction conditions have been established at 315º, with different wind intensities: 1) ff = 3.5 m/s, 2) ff = 7.1 m/s, 3) ff = 10.6 m/s, 4) ff = 14.1 m/s. In Fig. 25-28, the comparison of the accumulated precipitation field in twenty-four hours between each simulation and the control simulation is plotted on the left and the accumulated precipitation field with the wind field at 14 UTC is plotted on the right. For the wind field, a vector length of 1 cm (⟶) corresponds to 5 m/s, 7.5 m/s, 10 m/s and 12.5 m/s for each Fig. 25-28 respectively.
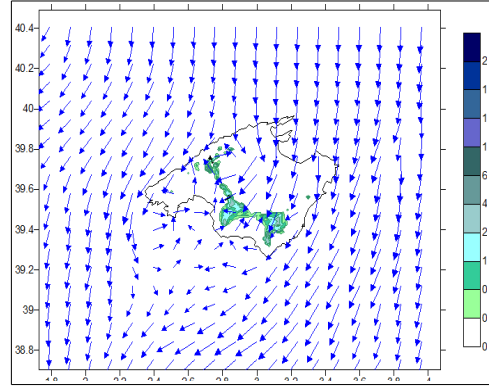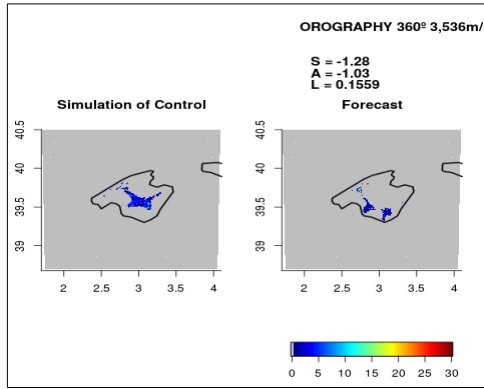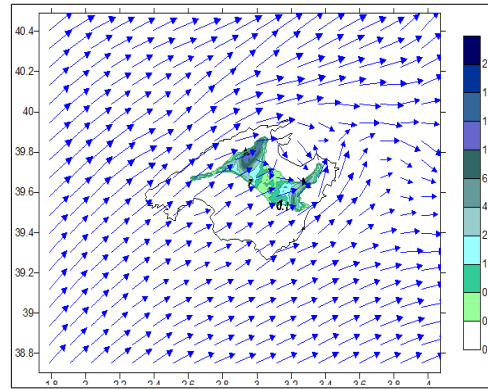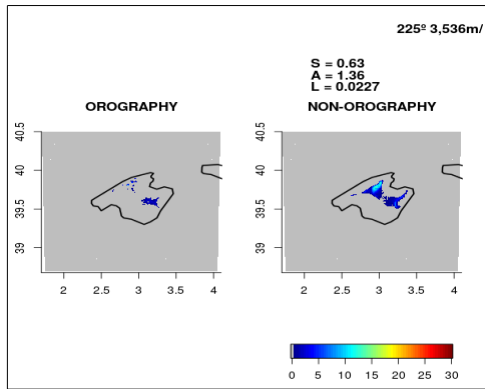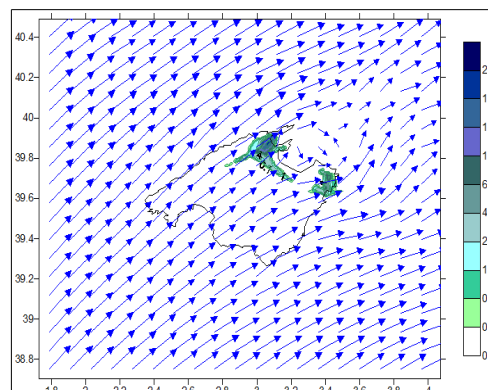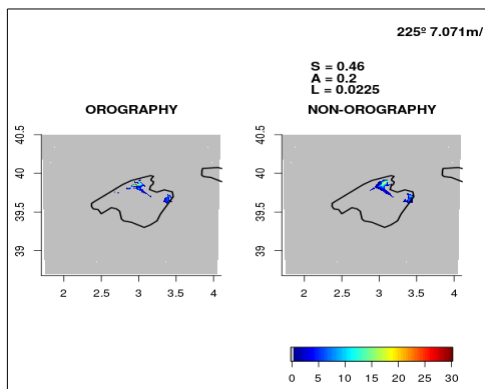
Figure 29
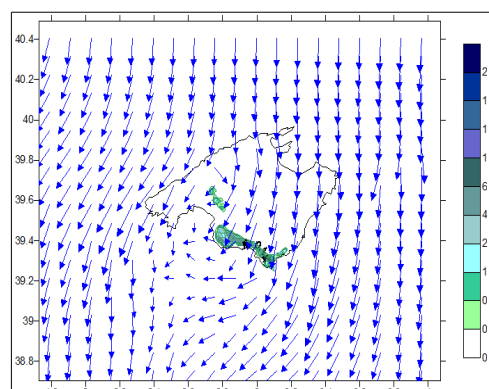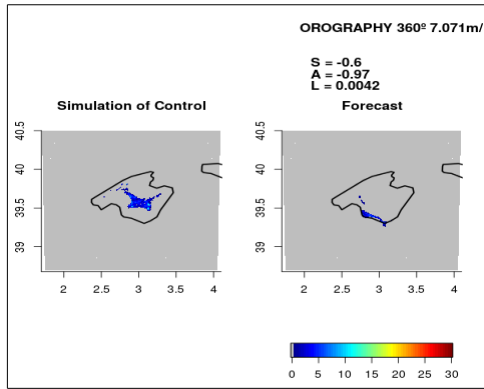
Figure 30
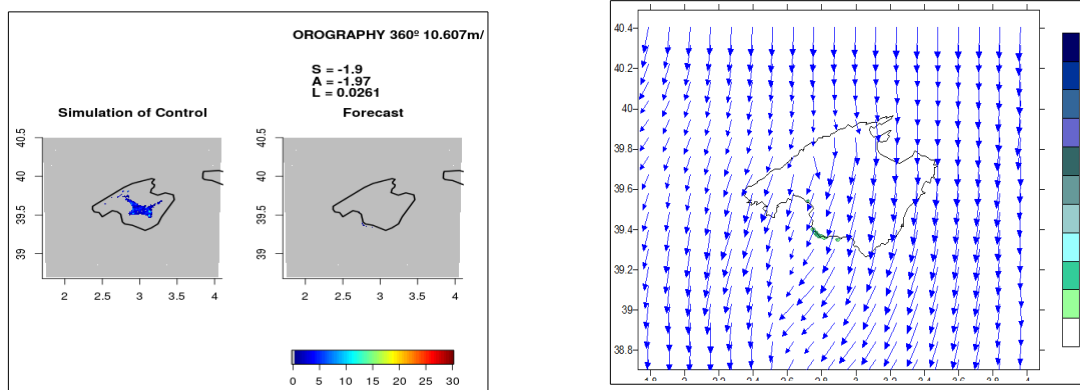
Figure 31
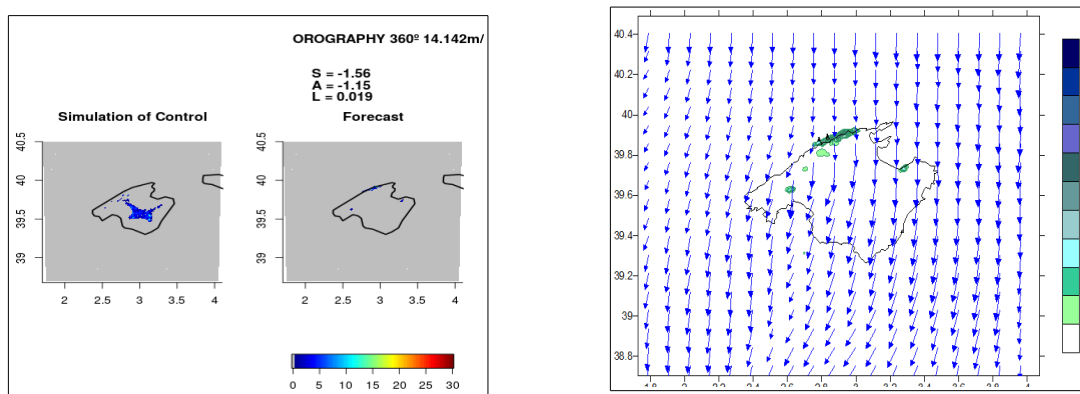
Figure 32

The initial and boundary wind direction conditions have been established at 360º, with different wind intensities: 1) ff = 3.5 m/s, 2) ff = 7.1 m/s, 3) ff = 10.6 m/s, 4) ff = 14.1 m/s. In Fig. 29-32, the comparison of the accumulated precipitation field in twenty-four hours between each simulation and the control simulation is plotted on the left and the accumulated precipitation field with the wind field at 14 UTC is plotted on the right. For the wind field, a vector length of 1 cm (⟶) corresponds to 5 m/s, 7.5 m/s, 10 m/s and 12.5 m/s for each Fig. 29-32 respectively.

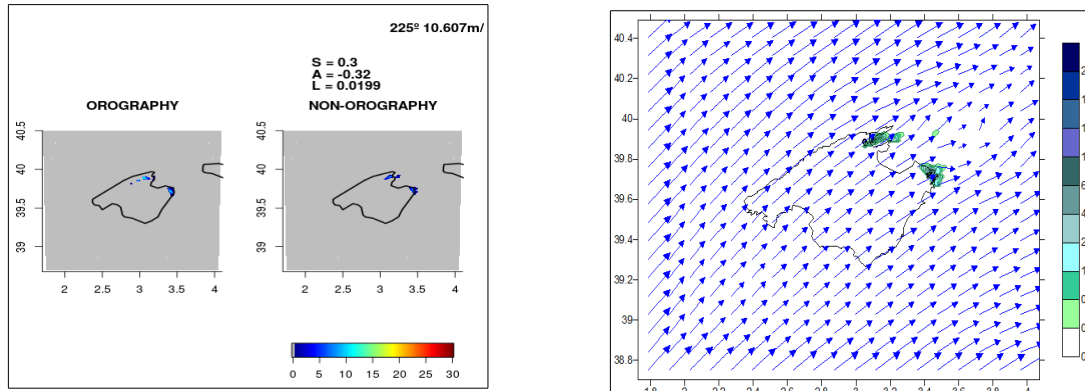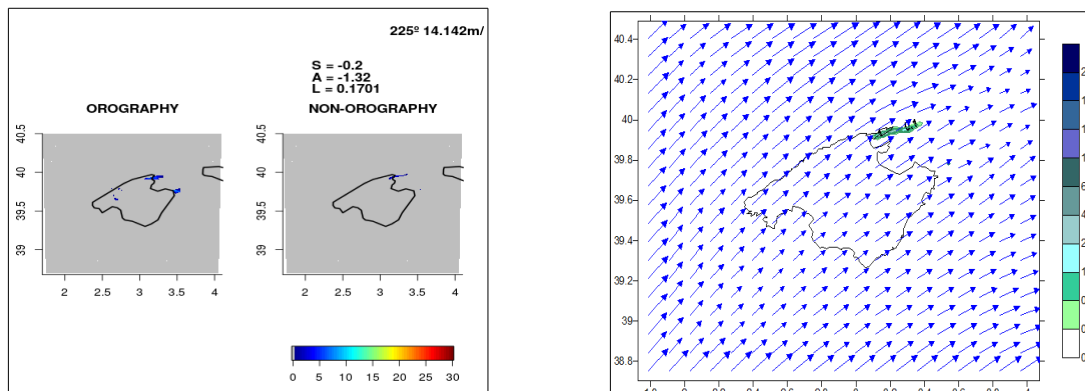# SIMULATIONS WITHOUT OROGRAPHY
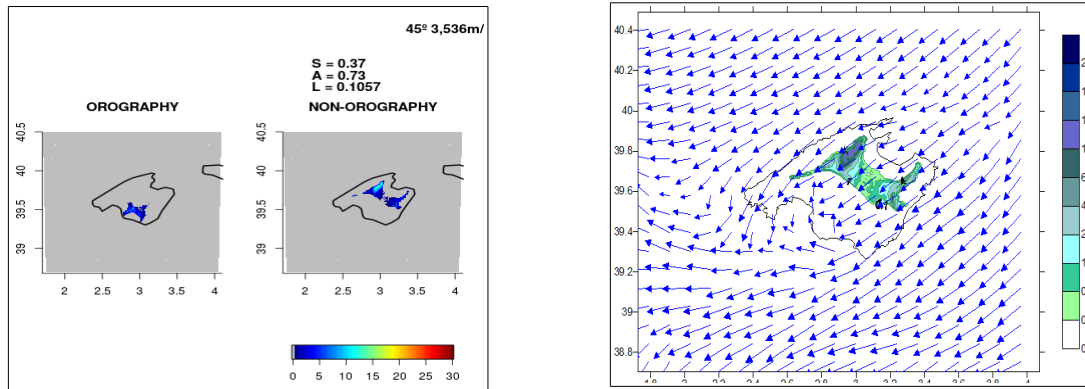
Figure 33
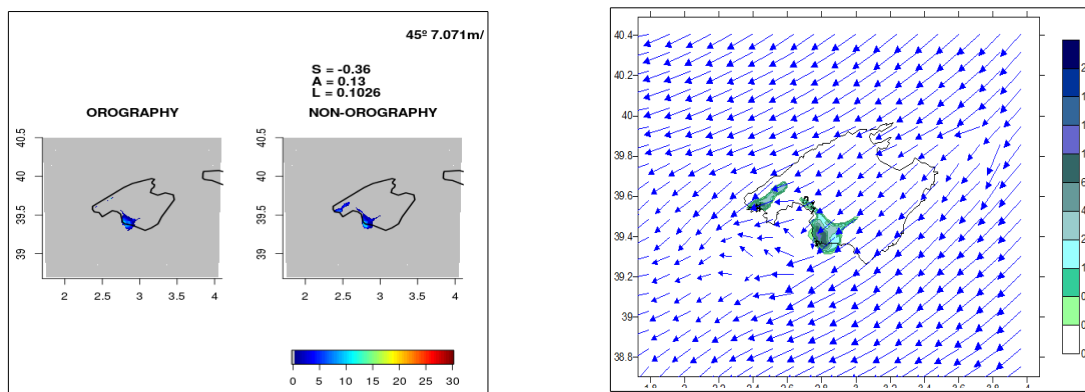
Figure 34
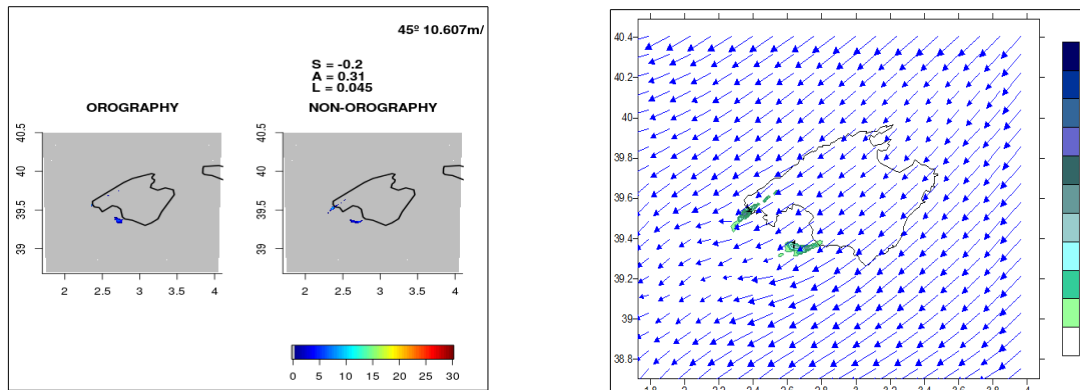
Figure 35
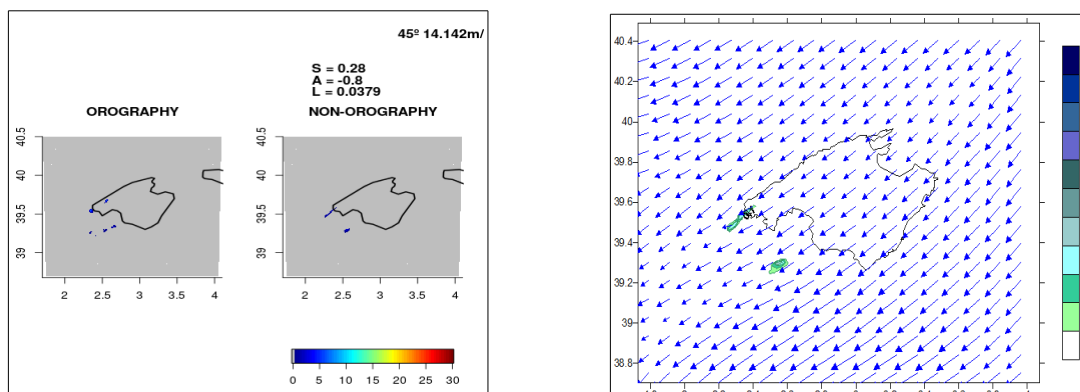
Figure 36

The initial and boundary wind direction conditions have been established at 45º, with different wind intensities: 1) ff = 3.5 m/s, 2) ff = 7.1 m/s, 3) ff = 10.6 m/s, 4) ff = 14.1 m/s. In Fig. 33-36, the comparison of the accumulated precipitation field in twenty-four hours is plotted on the left, for each simulation with non-orography with his counterpart with orography. The accumulated precipitation field for the simulation non orography and the wind field at 14 UTC are plotted on the right. For the wind field, a vector length of 1 cm (⟶) corresponds to 5 m/s, 7.5 m/s, 10 m/s and 12.5 m/s for each Fig. 33-36 respectively.
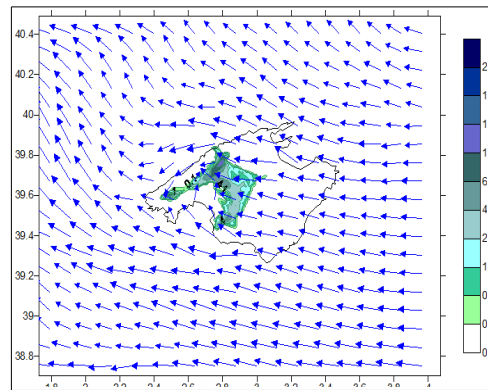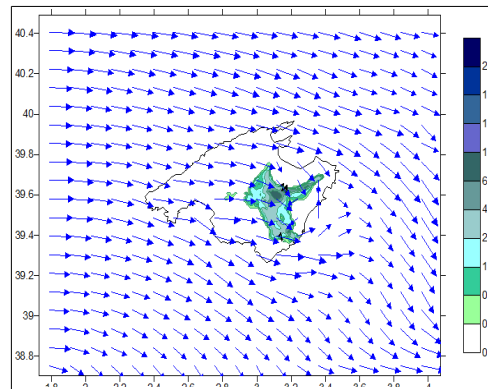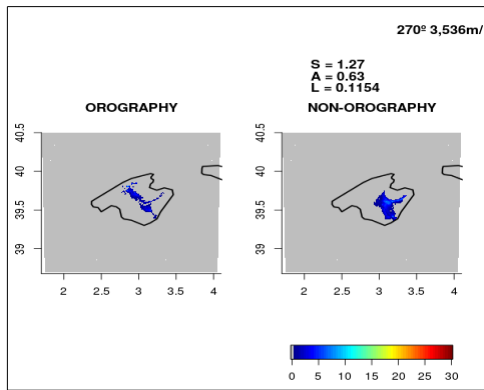
Figure 37

Figure 38

Figure 39

Figure 40

The initial and boundary wind direction conditions have been established at 90º, with different wind intensities: 1) ff = 3.5 m/s, 2) ff = 7.1 m/s, 3) ff = 10.6 m/s, 4) ff = 14.1 m/s. In Fig. 37-40, the comparison of the accumulated precipitation field in twenty-four hours is plotted on the left, for each simulation with non-orography with his counterpart with orography. The accumulated precipitation field for the simulation non orography and the wind field at 14 UTC are plotted on the right. For the wind field, a vector length of 1 cm (⟶) corresponds to 5 m/s, 7.5 m/s, 10 m/s and 12.5 m/s for each Fig. 37-40 respectively.

Figure 41

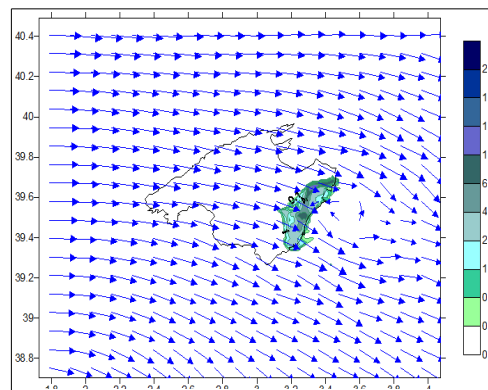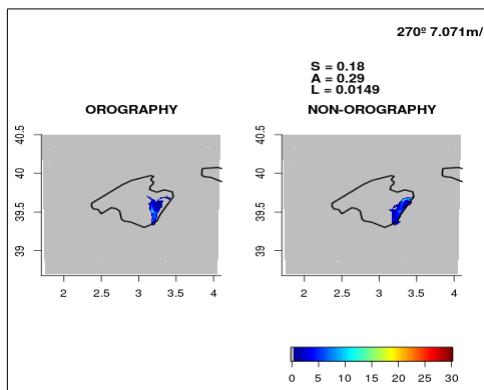Figure 42
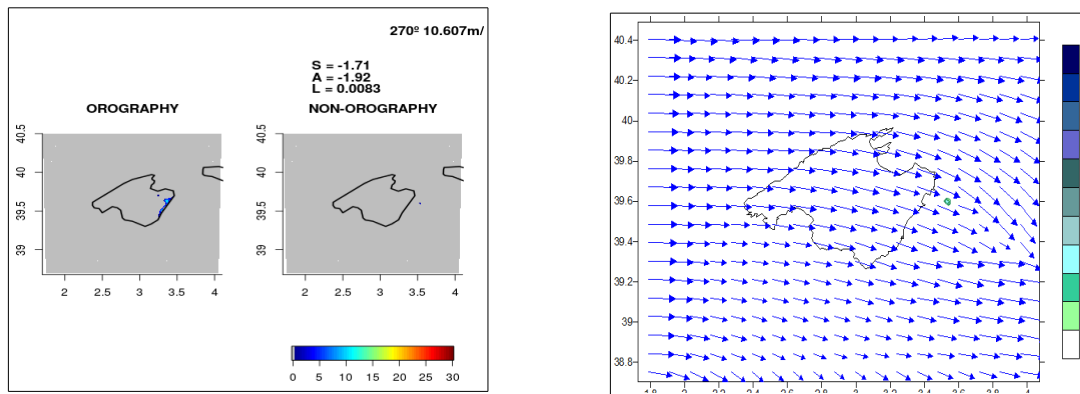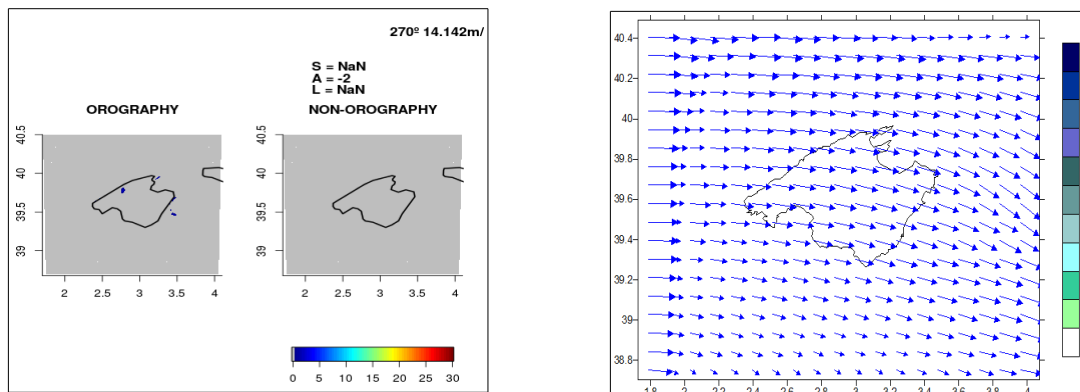
Figure 43

Figure 44

The initial and boundary wind direction conditions have been established at 135º, with different wind intensities: 1) ff = 3.5 m/s, 2) ff = 7.1 m/s, 3) ff = 10.6 m/s, 4) ff = 14.1 m/s. In Fig. 41-44, the comparison of the accumulated precipitation field in twenty-four hours is plotted on the left, for each simulation with non-orography with his counterpart with orography. The accumulated precipitation field for the simulation non orography and the wind field at 14 UTC are plotted on the right. For the wind field, a vector length of 1 cm (⟶) corresponds to 5 m/s, 7.5 m/s, 10 m/s and 12.5 m/s for each Fig. 41-44 respectively.
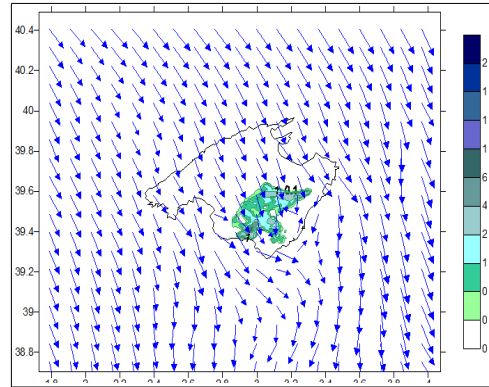
Figure 45

Figure 46

Figure 47

Figure 48

The initial and boundary wind direction conditions have been established at 180º, with different wind intensities: 1) ff = 3.5 m/s, 2) ff = 7.1 m/s, 3) ff = 10.6 m/s, 4) ff = 14.1 m/s. In Fig. 45-48, the comparison of the accumulated precipitation field in twenty-four hours is plotted on the left, for each simulation with non-orography with his counterpart with orography. The accumulated precipitation field for the simulation non orography and the wind field at 14 UTC are plotted on the right. For the wind field, a vector length of 1 cm (➝) corresponds to 5 m/s, 7.5 m/s, 10 m/s and 12.5 m/s for each Fig. 45-48 respectively.
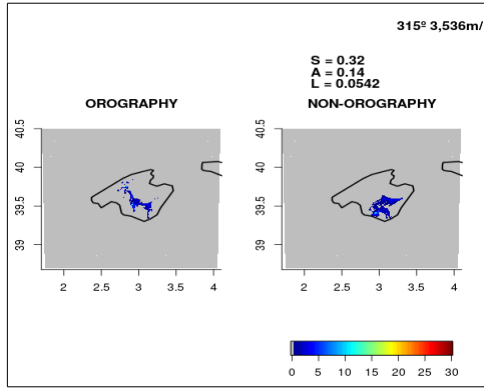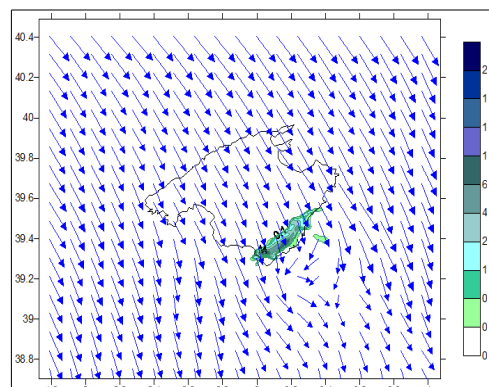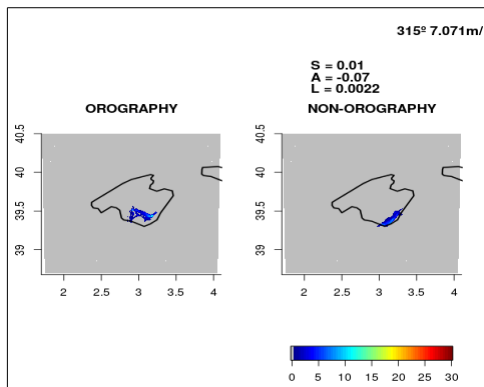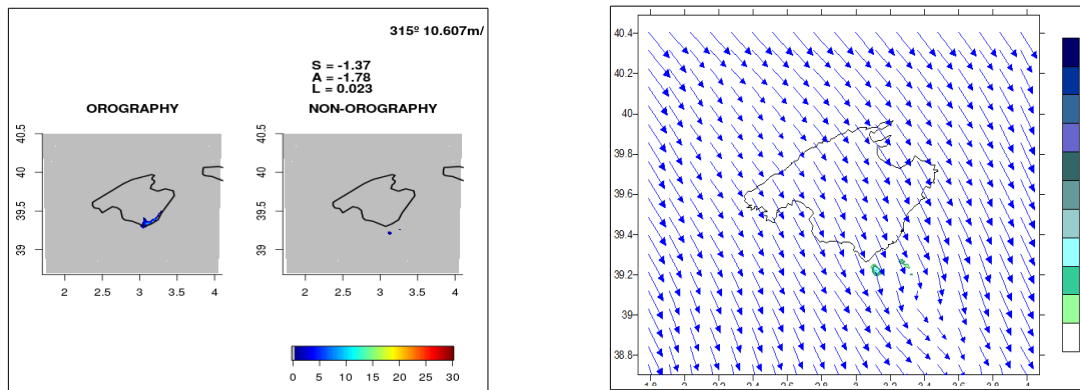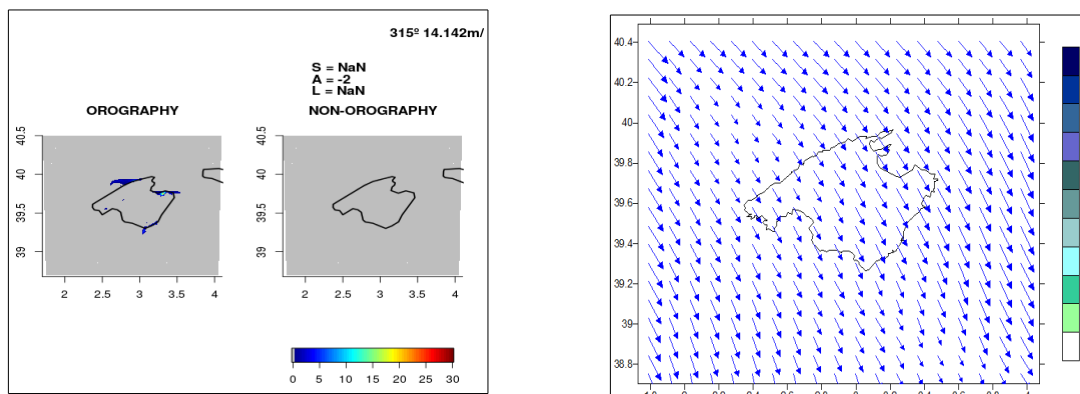
Figure 49

Figure 50

Figure 51

Figure 52

The initial and boundary wind direction conditions have been established at 225º, with different wind intensities: 1) ff = 3.5 m/s, 2) ff = 7.1 m/s, 3) ff = 10.6 m/s, 4) ff = 14.1 m/s. In Fig. 49-52, the comparison of the accumulated precipitation field in twenty-four hours is plotted on the left, for each simulation with non-orography with his counterpart with orography. The accumulated precipitation field for the simulation non orography and the wind field at 14 UTC are plotted on the right. For the wind field, a vector length of 1 cm (⟶) corresponds to 5 m/s, 7.5 m/s, 10 m/s and 12.5 m/s for each Fig. 49-52 respectively.

Figure 53

Figure 54

Figure 55

Figure 56

The initial and boundary wind direction conditions have been established at 270º, with different wind intensities: 1) ff = 3.5 m/s, 2) ff = 7.1 m/s, 3) ff = 10.6 m/s, 4) ff = 14.1 m/s. In Fig. 53-56, the comparison of the accumulated precipitation field in twenty-four hours is plotted on the left, for each simulation with non-orography with his counterpart with orography. The accumulated precipitation field for the simulation non orography and the wind field at 14 UTC are plotted on the right. For the wind field, a vector length of 1 cm (→) corresponds to 5 m/s, 7.5 m/s, 10 m/s and 12.5 m/s for each Fig. 53-56 respectively.
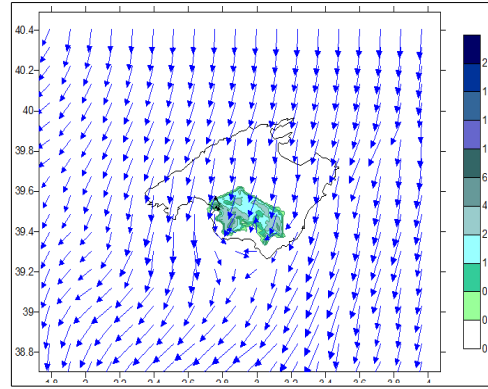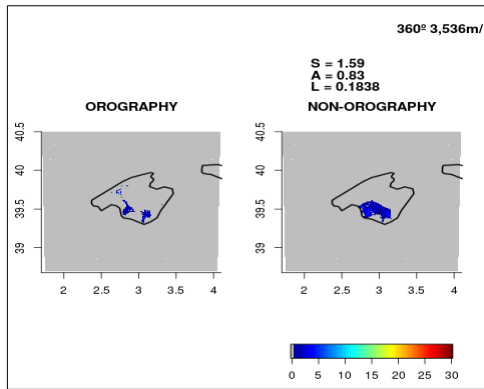
Figure 57

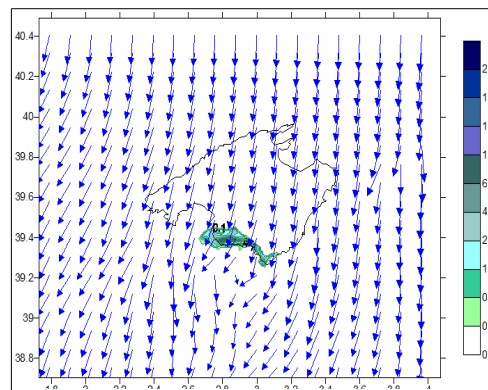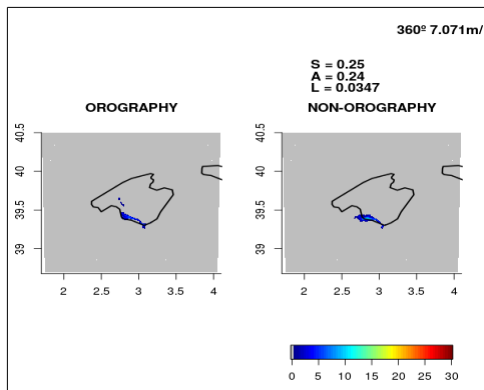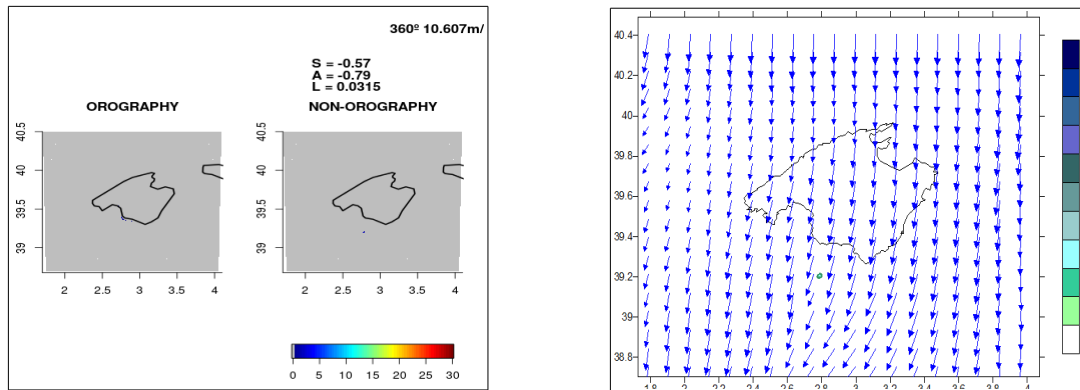Figure 58

Figure 59
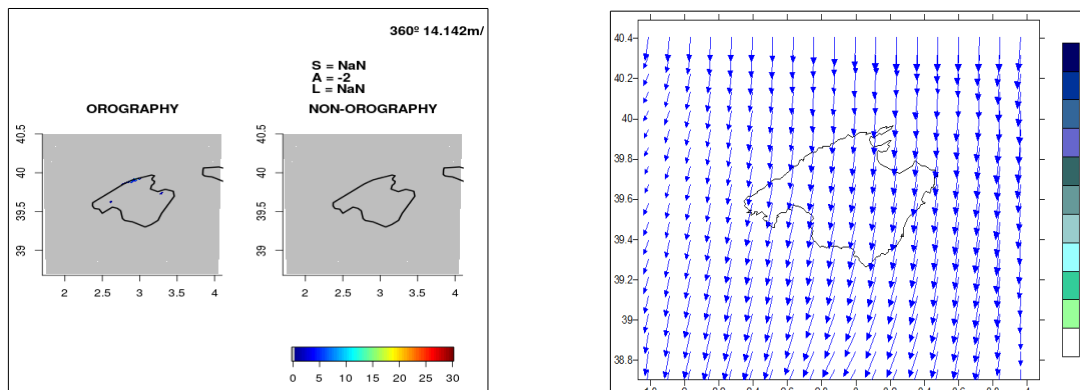

Figure 60

The initial and boundary wind direction conditions have been established at 315º, with different wind intensities: 1) ff = 3.5 m/s, 2) ff = 7.1 m/s, 3) ff = 10.6 m/s, 4) ff = 14.1 m/s. In Fig. 57-60, the comparison of the accumulated precipitation field in twenty-four hours is plotted on the left, for each simulation with non-orography with his counterpart with orography. The accumulated precipitation field for the simulation non orography and the wind field at 14 UTC are plotted on the right. For the wind field, a vector length of 1 cm (⟶) corresponds to 5 m/s, 7.5 m/s, 10 m/s and 12.5 m/s for each Fig. 57-60 respectively.

Figure 61

Figure 62

Figure 63

Figure 64

The initial and boundary wind direction conditions have been established at 45º, with different wind intensities: 1) ff = 3.5 m/s, 2) ff = 7.1 m/s, 3) ff = 10.6 m/s, 4) ff = 14.1 m/s. In Fig. 61-64, the comparison of the accumulated precipitation field in twenty-four hours is plotted on the left, for each simulation with non-orography with his counterpart with orography. The accumulated precipitation field for the simulation non orography and the wind field at 14 UTC are plotted on the right. For the wind field, a vector length of 1 cm ( ) corresponds to 5 m/s, 7.5 m/s, 10 m/s and 12.5 m/s for each Fig. 61-64 respectively.
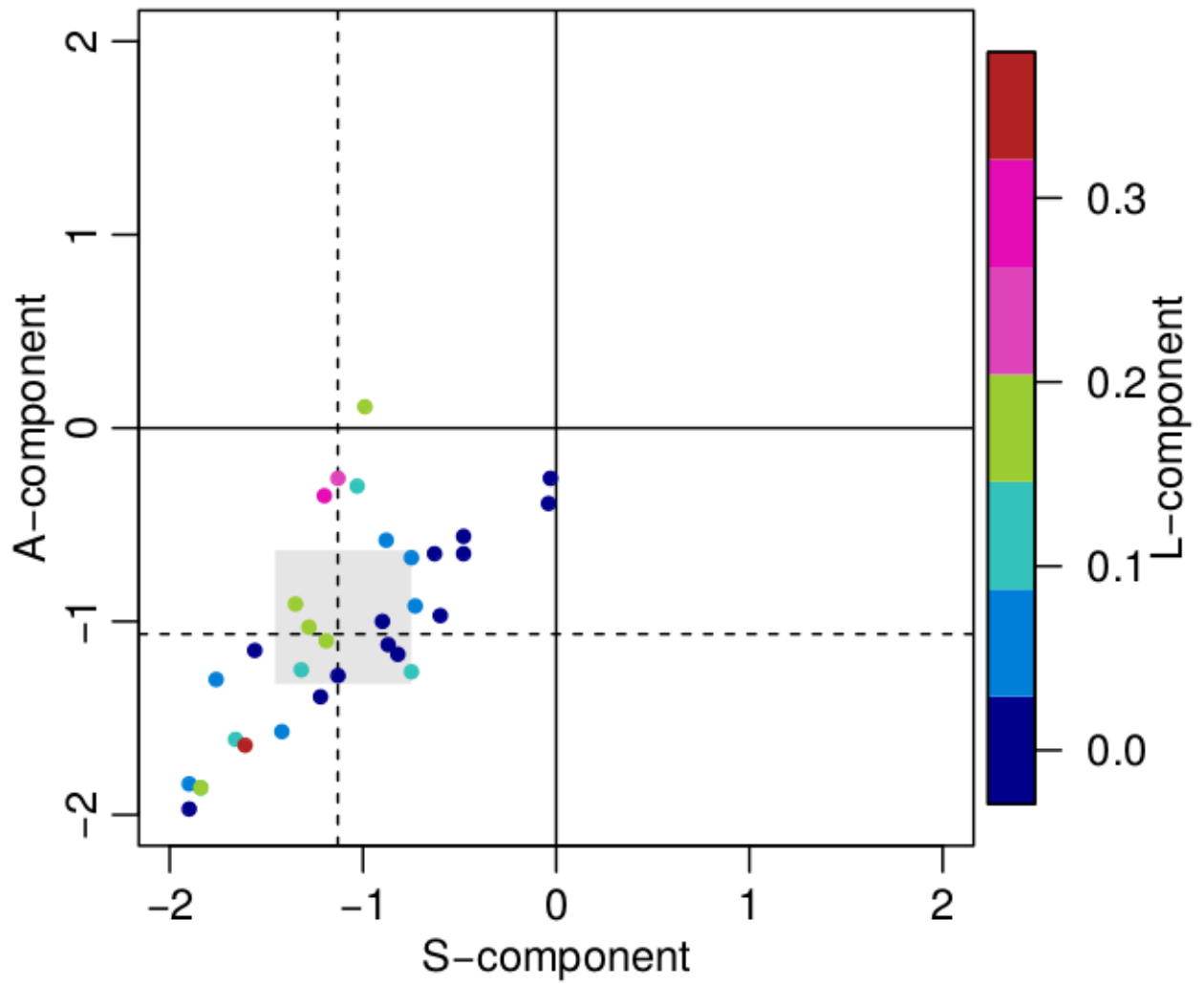
Figure 65. SAL diagram for accumulative precipitation field in 24 hours of the thirty-two scenarios. The orography is taking into account.
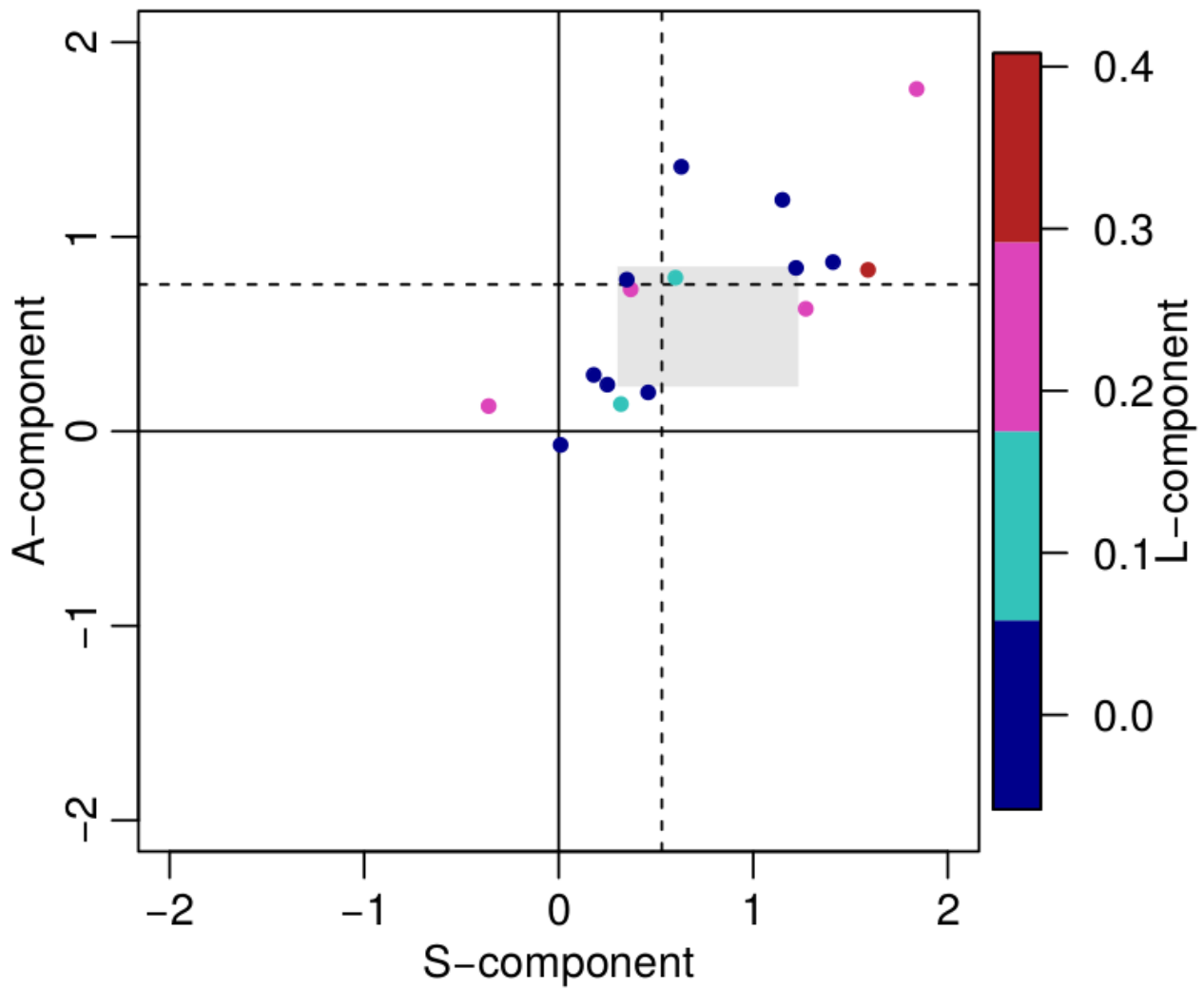
Figure 66. SAL diagram for accumulative precipitation field in 24 hours of the sixteen scenarios for wind speed intensities of 3.5 m/s and 7.1 m/s, the orography is set to zero.
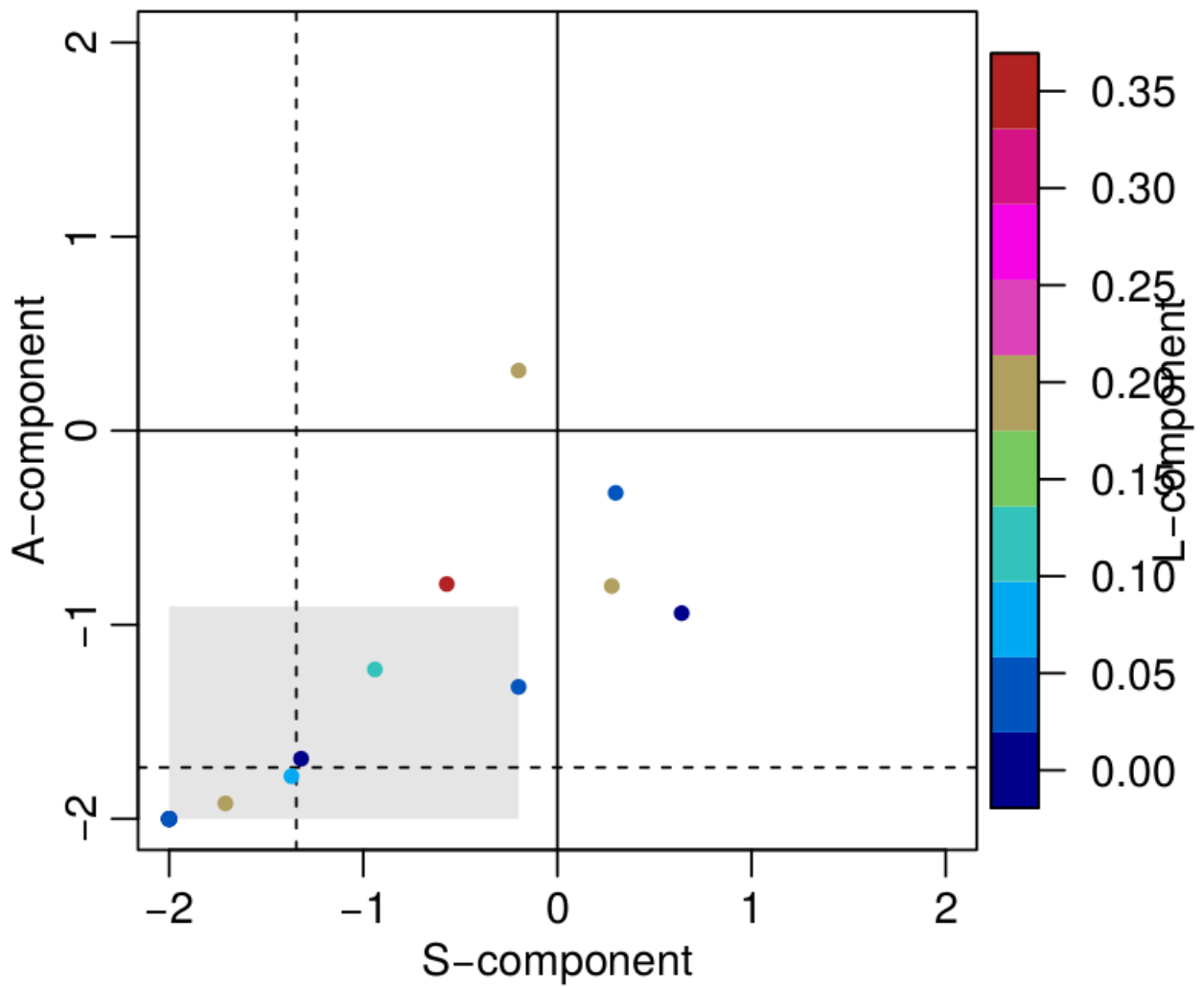
Figure 67. SAL diagram for accumulative precipitation field in 24 hours of the sixteen scenarios for wind speed intensities of 10.6 m/s and 14.1 m/s, the orography is set to zero.